A new approach for scaling beach profile evolution and sediment transport rates in distorted laboratory models.

Paul Maxime Bayle[1], *p.m.bayle@bath.ac.uk*, Tomas Beuzen[2], *t.beuzen@unsw.edu.au*, Christopher Edwin Blenkinsopp[1], *cb761@bath.ac.uk*, Tom E. Baldock[3], *t.baldock@uq.edu.au*, Ian Lloyd Turner[2], *ian.turner@unsw.edu.au*

[1] *Water Environment and Infrastructure Resilience Research Unit, Department of Architecture and Civil Engineering, University of Bath, Bath, BA2 7AY, United Kingdom*

[2] *Water Research Laboratory, School of Civil and Environmental Engineering, UNSW Sydney, NSW, 2052, Australia*

[3] *School of Civil Engineering, University of Queensland, St Lucia, Qld 4072, Australia*

Submission to: COASTAL ENGINEERING
Submission type: RESEARCH PAPER

ABSTRACT

Laboratory wave flume experiments in coastal engineering and physical oceanography are widely used to provide an improved understanding of morphodynamic processes. Wave flume facilities around the world vary greatly in their physical dimensions and differences in the resulting distortion of the modelled processes are reconciled using scaling laws. However, it is known that perfect model-prototype scaling of all hydro and morphodynamic processes is rarely possible and there is a lack of understanding to what extent distorted models can be used for direct morphological comparison. To address this issue, distorted scale laboratory flume experiments were undertaken in three different facilities, with the aim to measure and compare beach profile evolution under erosive waves and increasing water levels. A novel approach was developed to transform and scale the different experimental geometries into dimensionless coordinates, which enabled a direct quantitative comparison of the beach profile evolution and sediment transport rates between the differing distorted experimental scales. Comparing results from the three experiments revealed that the dimensionless scaled morphological behaviour was similar after the same number of waves – despite very different degrees of model distortion. The distorted profiles appeared to be suitable for comparison as long as a modified version of the Dean number is maintained between them. The new method was then validated with two further published datasets, and showed good agreement for both dimensionless profile shape, dimensionless sediment transport and morphodynamics parameters. The new approach scales the sediment transport by the square of the runup, proportional to HL, rather than H^2, and yields good agreement between the datasets. It is further shown that the new scaling method is also applicable for comparing distorted profile evolution under water level increase, as long as the water level is raised in a similar way between the experiments and by the same total increment relative to the significant wave height ($\Delta h/H_s$).

Keywords: *Scale modelling; Distorted profiles; Flume; Water Level Change; Morphodynamics.*

1. INTRODUCTION

Physical models have been widely used in coastal engineering to study complex coastal processes. Such models enable researchers to overcome the inherent obstacles of modelling coastal systems, such as large spatiotemporal timescales and natural variability, and to reproduce conditions in a controlled environment to better understand coastal processes [1]. In coastal engineering and physical oceanography, laboratory wave flumes (hereafter referred to simply as "flumes") have been extensively used to model beach profile evolution under wave forcing. Flumes exist in many laboratories around the world, ranging from prototype scale (100s metres long) to reduced-scale (a few metres long). One of the main challenges when undertaking laboratory experiments is how to correctly relate the observations and results from one experiment to another, and how to relate small-scale experiments to the prototype scale (*i.e.,* nature).

The number of previous studies that are available to perform scaling comparisons between different size flumes is limited. Indeed, every flume experiment has particular objectives and therefore uses specific experimental procedures and test cases to achieve them. For this reason, it is difficult to identify experiments from the literature with similar datasets which allow a complete and unbiased scale comparison. To the authors' knowledge, the only study performing such a comparison was undertaken by Van Rijn et al. (2011) [2] in which three similar experiments (with the same wave conditions and procedures) from three different flumes were quantitatively and qualitatively compared. It was shown that the morphodynamics of the different flume experiments at different scales could be compared as long as the scaled models were undistorted relative to each other (*i.e.,* scaling rules respected). However, the undistorted experiments compared in the work reported by Van Rijn et al. (2011) [2] were performed in the Hannover, Barcelona and Delft wave flumes, which are relatively large compared to the more common flume sizes that are available to most researchers. As a result, it remains unclear to what extent a comparison can be done between smaller scale flume experiments and prototype, distorted or not.

During the past several decades, many flume-based experiments have been undertaken to investigate beach and dune response to erosive and accretive waves, under monochromatic, bichromatic and random waves (*e.g.,* [3, 4]). These types of experiments have mainly been undertaken in small and medium flumes due to the relatively small number of large-scale flumes that are available to researchers around the world. More recently, flume experiments have been used to assess the impact of rising water levels on sandy coastline evolution to better understand the potential impacts of sea level rise caused by predicted climate change [5]. In particular, two medium-scale experiments, described in Atkinson et al. (2018) [6] and Beuzen et al. (2018) [7], have investigated beach profile response to erosive waves and a rising water level to study the effect of sea level rise on both engineered and non-engineered coastlines. While these two studies provided new insights into beach profile evolution under rising water levels, the scaled nature of the experiments means that the direct application of these flume-based observations to prototype scale behaviour is unclear.

This paper aims to develop a new scaling methodology for comparing beach profiles of distorted experiments, using three different datasets: a novel prototype-scale laboratory dataset (obtained as a component of the DynaRev experiment [8]), and two existing medium-scale model datasets (obtained from the experiments described in Atkinson et al. (2018) [6] and Beuzen et al. (2018) [7]). While each dataset measures beach profile response to erosive waves and increasing water levels, they differ in terms of scale and hydrodynamics. The proposed scaling method is used to analyse the morphological changes and sediment transport pattern of the three experiments under both still and increasing water level, in order to more comprehensively assess the potential and the limitations of the method.

Section 2 provides a summary of the most commonly used physics-based approaches to physical model scaling. Section 3 presents the three experiments used in this study and describe the parameters

used in the comparison. Section 4 compares the scale of each experiment and presents a novel approach to scale and compare distorted beach profiles. Section 5 presents the results and the validation of the profile comparison performed with the novel method, under still and increasing water level. Section 6 discusses the constraints associated with the method, and presents a one simple application of the new approach.

2. SCALING RULES FOR PHYSICAL MODELLING

The most common approach to scale a physical experiment is to use scaling laws in which the ratio of a parameter in the prototype and scaled model [3, 2] is expressed as follows:

$$n = \frac{p_p}{p_m} \tag{1}$$

where p_p represents the parameter in the prototype and p_m the same parameter in the scaled model (this is not limited to prototype, as two models can be compared to each other). This ratio is used in scaling laws, which are generally well established even though they often differ slightly from one author to another [9, 10, 11, 2]. For free surface flows dominated by gravity effects, hydrodynamic parameters are most commonly scaled using the Froude scaling law which assumes that the Froude number at model and prototype-scale is conserved. This law is represented by:

$$n_H = n_L = n_T^2 = n_h = n_u^2 \tag{2}$$

where *H* is the wave height, *L* the wavelength, *T* the wave period, *h* the water depth (if finite depth wave conditions are used) and *u* is the wave orbital velocity. This relationship ensures that the hydrodynamics of the scaled model are physically consistent with the prototype, and if Froude scaling is respected then the model hydrodynamics can be considered to be undistorted.

To verify the physical (geometrical) relationship between model and prototype, the distortion scale ratio is used [9, 10, 2], and defined as:

$$n_g = \frac{n_l}{n_h} \tag{3}$$

where n_g is the distortion scale ratio for physical geometry, n_l is the ratio of length and n_h the ratio of height between model and prototype. In the present context, these parameters usually represent the length and the height of the beach profile being analysed. If the result of Eq. 3 is unity, then the physical geometry of the model is undistorted (*i.e.,* same beach slope), otherwise, it is distorted.

While Froude scaling (Eq. 2) must be respected in a model to scale hydrodynamic parameters correctly, the distortion scale ratio (Eq. 3) is often considered to be a more flexible parameter. Noda (1972) [9] and Vellinga (1982) [3] defined different accepted ranges of distortion for this parameter as $n_l/n_h=(n_h)^{0.32}$ and $n_l/n_h=(n_h)^{0.28}(n_{ws})^{-0.56}$ respectively (*ws* being the sediment settling velocity) — the range being bounded by this value and 1. These two methods give the same order of magnitude for the accepted range of distortion, in which models are assumed to be qualitatively and quantitatively comparable to the prototype, as long as the Froude scaling is respected. Van Rijn et al. (2011) [2] also defined an accepted distortion range for both dune and beach erosion experiments. It has been argued that distorted models can be used if the qualitative behaviour of the beach profile is the most important feature, and not the precise quantitative reproduction of hydro and morphodynamics [3, 2, 12, 6].

Other parameters have been identified [1, 13, 14, 2] as important for model scaling, and they are presented in Table 1, along with their generally accepted thresholds. Following the aforementioned

scaling laws, two experiments which are undistorted regarding the Froude and geometry scaling automatically have the same surf similarity (ξ_0) and wave steepness (H/L) parameters. However, these laws do not consider the sediment size and type, which are two important parameters incorporated into the dimensionless fall velocity (also referred to as the "Dean number", [15, 16]), the Shields's number and the Reynolds number (see Table 1). As a result, an additional scaling parameter n_{D50} has been taken into consideration in many studies [9, 10, 2]. According to these studies, various authors have suggested acceptable ranges within which results can be considered comparable to prototype and have defined some rules to scale it ($n_{D50} = (n_h)^{0.83}$ for $n_h < 2.2$ and $n_{D50} = 1.7(n_h)^{0.2}$ for $n_h \geq 2.2$, in Van Rijn (2011) [2]). Generally, the sediment diameter is scaled so that the excess of bed shear stress or friction velocity are the same in all experiments — *i.e.,* the difference between the actual bed shear stress at a given depth and the critical value required to initiate motion is the same for all experiments. As a result, if Froude scaling (Eq. 2) is respected and the sand is correctly scaled, then the Shields's and Dean number are maintained between prototype and model, but the grain Reynolds number is not. This physical inconsistency is inherent to model scaling and means that the sand grain size always introduces scaling error, whether via the Shields's and Dean number or the Reynolds number. Furthermore, the modified version of the Dean number, including the slope, is only conserved if the compared experiments have the same initial slope. Therefore, using similar sand size in model and prototype and matching the modified version of the Dean number would automatically lead to a distorted model regarding the Froude scaling law.

Table 1: Important parameters to consider for scaling of coastal engineering models. H_0 is the deepwater significant wave height (m), *Tp* the wave peak period (s), L_0 is the associated deepwater wavelength (m), β is the beach slope angle, w_s is the sediment settling fall velocity (m/s), $\tau_0(d)$ is the bed shear stress (N/m^2) at the depth *d* (m), ρ_s and ρ are respectively the sediment and water density (kg/m^3), *g* is the acceleration due to gravity (m/s^2), D_{50} is the median sediment diameter (m), u_* is the friction velocity (m/s) and ν is the kinematic viscosity (m^2/s). The lower case "0" indicates deepwater wave condition for the rest of the paper. The lower case 'crit' indicates the critical value of the parameter.

Parameter name	**Parameter symbol**	**Equation**	**Threshold**
Surf similarity parameter or Iribarren number	ξ_0	$tan\beta \,/\, \sqrt{\frac{H_0}{L_0}}$	$\xi_0 < 0.3$, Dissipative $0.3 < \xi_0 < 1$, Intermediate $\xi_0 > 1$, Reflective
Dimensionless fall velocity [15, 16]	Ω_0	$\frac{H_0}{w_s T_p}$	$\Omega_0 < 1$, Reflective $1 < \Omega_0 < 6$, Intermediate $\Omega_0 > 6$, Dissipative
Modified dimensionless fall velocity [17]	Ω_β	$\frac{H_0 tan\beta}{w_s T_p}$	$\Omega_\beta < 0.08$, Onshore transport dominates. $\Omega_\beta > 0.08$, Offshore transport dominates.
Shields's number [18]	$\theta_0(d)$	$\frac{\tau_0(d)}{(\rho_s - \rho) g D_{50}}$	$\theta_0(d) > \theta_{crit,bedload}$, Bedload transport expected at depth *d.* $\theta_0(d) > \theta_{crit,susp}$, Suspension transport expected at depth *d.*
Wave steepness	W_{st}	H_0/L_0	-
Grain Reynolds number	$R_{e*}(d)$	$\frac{u_* D_{50}}{\nu}$	$R_{e*}(d) > R_{e,crit}$, Inertia force is strong enough at depth *d.* $R_{e*}(d) < R_{e,crit}$, Inertia force is not strong enough at depth *d,* which limits bedload transport.

Besides this paradox, sand scaling is not performed in many laboratory experiments for two primary reasons: firstly, for practicality and reduced operational costs, flumes tend to have a permanent type of sand regardless of the experiment; and, secondly, for small scale models, the theoretical scaled sand diameter would be so small that it would have cohesive properties which would significantly influence sediment transport behaviour. Indeed, according to the Shields entrainment function [18], the critical Shields's number required to initiate motion significantly increases for sediment characterised by a critical Reynolds number smaller than 2. Moreover, according to the initiation of suspended sediment transport curve [19, 20], sediment with a dimensionless grain number smaller than 3 do not undergo bedload transport but instead, switches directly from immobile to suspended. For these reasons, lightweight (often artificial) sediment has been used in many experiments in the past.

Based on existing scaling rules, a model can be undistorted in one aspect (*e.g.,* hydrodynamics) but distorted in another (*e.g.,* geometric scale). Previous laboratory studies have mainly focused on models which are distorted with respect to sediment size only [2] — not respecting the sediment scaling rules, but respecting the geometric and/or Froude scaling — but little attention has been given to models distorted with respect to hydrodynamics (Froude scaling) or physical geometry (distortion scale ratio), or both. As a result, the suitability of such models to be used for qualitative and quantitative comparisons has not been thoroughly assessed.

To relate the morphological changes observed in a model to the prototype, it is important to compare the data at the same relative time using existing scaling rules (*e.g.,* $n_{TM} = (n_h)^{0.5}$; [2, 11]). However, these rules are only applicable if the compared experiments have the same distortion scale ratio n_g (or at least within the accepted range of distortion) and if the hydraulic Froude scaling is respected. In consequence, it is complicated to scale time for models which are distorted regarding these latter rules. To overcome this issue, a common approach is to compare profiles after the same number of waves. This does not remove completely the time component from the analysis, as it is equivalent to a hydrodynamic time instead, but it is generally accepted as a good approximation [9, 11].

In addition to considering scale effects in laboratory models, it is crucial to have a reliable methodology to compare a modelled profile with the prototype. One approach is to convert the local coordinate of each profile in the laboratory setting into dimensionless coordinates shared by both scales. Van Rijn et al. (2011) [2] attempted this by multiplying the local profile coordinate by the square of the local offshore significant wave height (H_{m0}), which is appropriate if the model is not distorted with respect to geometry (*e.g.,* same beach slope). Here we propose that for distorted models, a similar approach can be employed using the method adopted by Peregrine and Williams (2001) [21] for swash flows. Peregrine and Williams (2001) [21] used parameters shown in Eq. (4) and Eq. (5) to remove beach gradient and non-dimensionalise the non-linear shallow water equation for swash flows:

$$x^* = \frac{(sin\beta)x}{A} \tag{4}$$

$$z^* = \frac{(cos\beta)z}{A} \tag{5}$$

where β is the angle of the beach slope, x and z are the local coordinate system, x^* and z^* are the new dimensionless coordinate system, and A is half of the length of the vertical excursion of the undisturbed swash, measured from the lower boundary of the swash to the maximum height of run-up. These two equations (Eq. 4 and Eq. 5) appear more suitable for the analysis of distorted profiles as they rotate all profiles onto the same 45^o gradient (*e.g.*, [22]). This scaling does not however relate the coordinate system to the offshore wave conditions of each experiment and this paper also provides the method to address this.

3. METHODOLOGY

3.1 Wave flume and instrumentation

The methodology presented in this paper for comparing distorted datasets was developed from two scaled model datasets and a prototype-scale dataset obtained in three different laboratories. The details of each wave flume are presented here and summarised in Table 1.

The prototype-scale dataset was obtained from the DynaRev experiment, which was undertaken in the Groβer WellenKanal (GWK) large wave flume laboratory, during August and September 2017. The flume is located at the Forschungszentrum Kuste (FZK Coastal Research Centre), which is a joint institution between the University of Hannover and the Technical University Braunschweig located in Hannover, Germany. A complete experimental description can be found in Blenkinsopp et al. (*in review*) [8] and further details of the experiment are presented in Bayle et al. (*2020*) [23]. The flume is 309 m long, 7 m deep and 5 m wide and equipped with a combined piston-flap-type wave paddle. Reflected waves and low-frequency resonance (*e.g.,* seiche) are damped at the paddle using Automatic Reflection Compensation (ARC). A mechanical profiler was used to measure the beach profile after each test. The profiler consists of a mechanical roller attached to a mobile trolley which runs along the flume sidewalls. It measures the bed coordinates, within 1-2 cm of vertical and horizontal accuracy. The coordinate system is defined as follows: the cross-shore position, x has its origin at the wave paddle and is positive toward the beach; the vertical elevation, z is positive upward the concrete bottom of the flume.

The first scaled model dataset was obtained from an experiment performed in the University of New South Wales (UNSW) flume located at the Water Research Laboratory (WRL), Sydney, Australia. The complete experimental description and results can be found in Beuzen et al. (2018) [7]. This flume is 44 m long, 1.6 m deep and 1.2 m wide. It uses a piston-type wave paddle backed with specialised foam blocks to damp wave reflections. Beach profiles were measured using a laser measurement system, as described in Atkinson and Baldock (2016) [24]. This system consists of an array of five SICK DT50-P111 class 2 laser distance sensors mounted above the flume on a trolley rolling on the flume sidewall. The final measured profile is an average of the five cross-shore profiles obtained and is measured within 2 mm of vertical and horizontal accuracy. The coordinate system is defined as follows: the cross-shore position, x has its origin at the bottom of the beach profile and is positive toward the beach; the vertical elevation, z is positive upward the bottom of the flume.

The second scaled model dataset was obtained from an experiment undertaken in the University of Queensland (UQ) flume at the School of Civil Engineering, Brisbane, Australia. The flume is 22 m long, 1 m deep and 1 m wide, a complete description is given in Baldock et al. (2017) [25]. The flume has a piston-type wavemaker with active wave absorption. Beach profiles were obtained using the original laser measuring system developed by Atkinson and Baldock (2016) [24]. It measures the bed coordinates within 2 mm of vertical and horizontal accuracy. The coordinate system is defined as follows: the cross-shore position, x has its origin at the wave paddle and is positive toward the beach; the vertical elevation, z is positive upward the bottom of the flume.

Table 2: Size of the three physical laboratory flumes used in this paper, along with the general test conditions and characteristics for each experiment.

	Length (m)	**Width (m)**	**Height (m)**	**H_s (m)**	**T_p (s)**	**Slope**	**Sand D_{50} (mm)**	**Water Level (m)**	**Time at each water level (h)**
GWK	309	5	7	0.8	6	1:15	0.33	4.5 4.6 4.7 4.8 4.9	20 7 7 7 14
UNSW	44	1.2	1.6	0.15	1.25	1:10	0.35	1 1.015 1.030 1.045 1.060 1.075	7.67 4.67 3 3 3 12.67
UQ	22	1	1	0.16	1.18	1:15	0.30	0.6 0.65	24 25

3.2 General test conditions

The details of the test conditions for the three experiments are presented and summarised in Table 2. The three experiments used in this paper had different purposes:

- GWK experiment: the primary aim was to test the coastal protection performance of a dynamic cobble berm revetment installed on a sandy beach under erosive waves and water level changes. The performance of the revetment was assessed by comparing beach profiles, shoreline retreat and runup with and without the structure under the same hydrodynamic forcing [8, 23]. The current paper primarily focusses on test cases with a sand-only beach (SB0 in [8]) except for section 6.2.
- UNSW experiment: this study compared beach profile evolution of an unprotected sandy beach and a sandy beach protected by a seawall or a revetment, under erosive waves and rising water level [7]. The current paper primarily focuses on the test case with a sand-only beach exposed to erosive waves and changing water level (E1 in [7]) except for Section 6.2.
- UQ experiment: this experiment investigated the response of beach profiles under erosive and accretive waves and water level changes to investigate the accuracy of the Bruun rule and derivatives [6]. The sandy beach tested was not protected. The results used here correspond to test E5 from Atkinson (2018) [26].

All three experiments investigated the response of a sandy beach profile under erosive wave conditions and with a rising water level. All started with a planar sandy beach profile, and the sand in each experiment was relatively similar in size and was non-cohesive in all cases. Based on the specified significant wave height and peak wave period, time series of irregular waves were generated using a JONSWAP spectrum, with a peak enhancement coefficient of 3.3. First-order wave generation was chosen for all experiments as each flume had a system to absorb the reflection and limit the propagation and impact of spurious waves. The different profiling systems do not affect the profile comparison as the measurement error associated with them is too small relative to the observed changes in bed elevation.

Beyond the scale of each flume experiment, there were a few other notable differences. GWK and UQ had the same initial beach slope (1:15) whereas UNSW had a steeper profile (1:10). Under a fixed

water level, the beach profiles were exposed to 20 hours, 7.67 hours and 24 hours of waves for GWK, UNSW and UQ respectively. Regarding water level changes, GWK and UNSW used a series of incremental water level rises (four steps for GWK and five steps for UNSW) for a total rise of 0.4 m and 0.075 m respectively, while UQ used a single step water level rise of 0.05 m. These two approaches for raising the water level were shown to give the same final beach profile, as long as enough time was allowed for the profile to reach a quasi-equilibrium [7]. As a result, intermediate profiles may not be comparable, but the end profiles should be. Finally, the profile evolution was surveyed at irregular and different time steps for each experiment.

3.3 Morphological parameters

The definitions of the beach profile morphological features used in the comparison of the three experiments are presented in Figure 1. The evolved beach profile is represented by a double bar system as this is the type of profile obtained in all the experiments used in this study. The offshore bar is referred to as the 'outer bar' and the onshore bar as the 'inner bar'. The distance between the crests of these two bars is used to define the size of the trough. The elevation of the bar and berm crest relative to the still water level is defined as z_{bar} and z_{berm} respectively. The elevation of the bar and berm crest above the initial profile is defined as h_{bar} and h_{berm} (not shown) respectively. The cross-shore position of the outer bar is defined relatively to the shoreline as x_{bar}. The most landward point on the beach where zero bed-level changed is measured over time is defined as x_0.

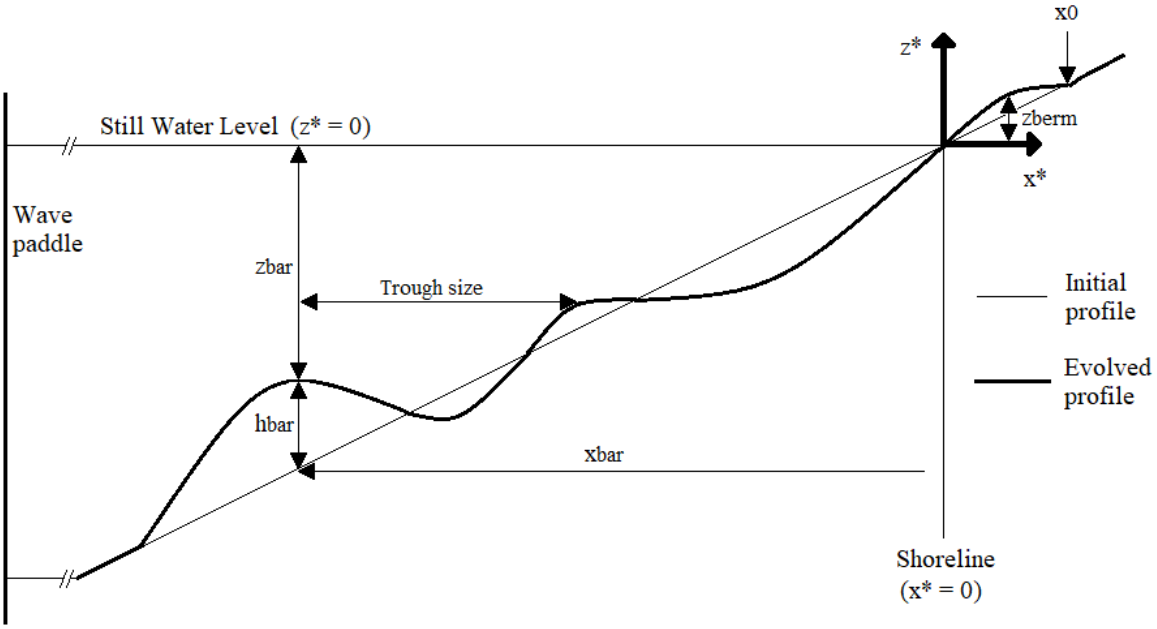

Figure 1: Definition of the morphological parameters used in this study. Note that the '*' refer to the dimensionless coordinate system (see section 4.2).

The main parameter used in this study to assess similarities and differences between experiments is the cross-shore sediment transport pattern. The local total sediment transport volume (bedload and suspended load) per unit width at a given cross-shore position x, q(x) (m^3/m), was defined at each time interval as the sum of the beach volume change relative to the initial planar profile, from the most landward point of the profile (x_0) to the point of interest (x):

$$q(x) = \int_{x}^{x_0} \Delta z(x) dx \qquad (6)$$

where x_0 is the landward location of no profile change (*i.e.*, $q(x_0) = 0$), Δz is the observed change in bed elevation (m) between the profile and the initial planar profile at location x and dx is the cross-shore increment (m). The bulk cross-shore sediment transport volume is defined as the integral of $q(x)$ over the same cross-shore limits [12, 27]. Closure errors in the integration ($q(x_{end}) \neq 0$, where x_{end} is the offshore limit of the active profile and the integration commences from the seaward limit (x_o)) can still occur due to unaccounted volume missed by the profile measurements, as well as variable sediment porosity and compaction. Closure errors were accounted for here following the methodology of Baldock et al. (2011) [12] by uniformly distributing any residual error through the active profile between x_0 and x_{end}. The offshore limit of the active profile, x_{end}, was extracted from the profile data as the offshore point where no significant change occurred over time. Extracted values were validated with the theoretical value of the depth of closure for each experiment.

4. SCALE ANALYSIS

4.1 Distortion analysis

The GWK experiment is considered to be at prototype scale, while the two other experiments are considered to be medium-scale. Although in the comparative analysis presented below, particular attention is given to the comparison of the medium-scale experiments with the prototype, the comparison of the two medium-scale models is also of interest. The parameters used to perform the scale analysis are shown in Table 3.

Table 3: Parameters used for the scale analysis. The names associated with the symbols are in Table 2.

	l (m)	h (m)	H_0 (m)	L_0 (m)	W_{st}	ξ_0	Ω_0	Ω_β	$\theta_0(d)$	$R_{e*}(d)$	$\frac{\Delta h}{H_s}$
GWK	60	4	0.838	56.20	0.015	0.55	3.38	0.24	0.269	12.52	0.5
UNSW	10	1	0.153	2.44	0.063	0.40	2.78	0.28	0.060	6.42	0.5
UQ	9	0.6	0.170	2.17	0.078	0.24	3.87	0.26	0.097	6.52	0.31

The horizontal length of the model, l corresponds to the cross-shore extent of the sand profile used in each flume [3, 2]. It represents the horizontal distance between the toe of the initial planar profile and the shoreline position at the initial water level. As the initial profile was planar for the three experiments, this directly relates to the gradient of the slope. The vertical height of the model, h corresponds to the still water level elevation above the toe of the initial planar profile. For UNSW and UQ, the planar slope ends directly on the bottom of the flume, such that the value of h is equal to the original water depth. However, for GWK where a 0.5 m high flat layer of sand was placed offshore of the planar profile, the value of h is smaller than the water depth. These parameters are used to calculate the distortion scale ratio n_g (Table 4) between the three experiments. GWK and UNSW have a distortion scale of $n_g = 1.5$ whereas GWK and UQ have a value of $n_g = 1$, so are not geometrically distorted. UNSW and UQ are distorted with a ratio of $n_g = 0.67$.

The offshore significant wave height, H_0 (Table 3) is obtained by deshoaling the significant wave height at the wave paddle to deep water using the linear wave theory. The corresponding offshore wavelength, L_0 (Table 3) is calculated using the peak wave period T_p (Table 2). The maximum wave orbital velocity U_{max} (not shown) at the offshore point of no change x_{end} (corresponding to water depths of 2.32 m, 0.4 m and 0.33 m deep for GWK, UNSW and UQ respectively) is obtained using the linear wave theory. These parameters along with h are used to assess the Froude scaling law for hydraulic comparison (Table 4). Froude scaling is not maintained between any of the experiments (see Equation 2). As a result, the offshore wave steepness differs for each experiment (Table 3), with UQ having the steepest waves and GWK the least steep.

Table 4: Froude scaling parameters (n_{H_0}, n_{L_0}, n_l, $n_{T_p}^2$, n_u^2 and n_h), and distortion scale n_g.

	n_{H_0}	n_{L_0}	$n_{T_p}^2$	n_h	n_l	n_u^2	n_g
GWK-UNSW	5.46	23.04	23.04	4	6	11.63	1.5
GWK-UQ	4.93	25.85	25.85	6.67	6.67	7.13	1
UNSW-UQ	0.90	1.12	1.12	1.67	1.12	0.61	0.67

As suggested by Vellinga (1986) [11], Baldock et *al*. (2010) [14] and Van Rijn et *al*. (2011) [2], the surf similarity parameter or Iribarren number, ξ_0 was calculated (Table 3). The Iribarren number for the GWK experiment characterises an intermediate beach state with plunging waves [28, 29]. For UNSW, it characterises an intermediate beach state with spilling waves and for UQ, it characterises a dissipative beach state with spilling waves.

The settling fall velocity of sand used in the calculation of the Dean number and its modified version (see Table 1) was 0.041, 0.044 and 0.037 m/s for GWK, UNSW and UQ respectively. Although the Dean numbers (Ω_0) differ between each experiment, they all fall within a range which is characteristic of an intermediate beach profile. The modified version (Ω_β) is more interesting when dealing with scale comparison as it also takes into account the initial beach slope. Therefore, as explained in Baldock et *al*. (2010) [14], this allows the slope to be linked directly to the grain size, with a steep slope and coarse grain size being comparable to a gentle slope and fine grain size. In the current study, UNSW has the largest value of Ω_β while UQ and GWK have slightly smaller values (see Table 3). Note that UNSW has a steeper slope, but also the coarser sand.

The Shields and Reynolds number are both calculated at $x = x_{end}$, which is near the back of the bar. The UNSW and UQ Shields's number are significantly smaller than for the GWK (Table 3), however all are above the critical value for initiation of motion ($\theta_{crit,bedload}$ is equal to 0.038, 0.0375 and 0.0403 for GWK, UNSW and UQ respectively). Note however that only GWK is significantly above the critical value for suspended transport, with $\theta_{crit,susp} \approx 0.08$ for the three experiments. As a result, morphological changes and sediment transport behaviour seaward of the bar crest are expected to be different for UNSW and UQ, as sediment transport in this area will mostly consist of bedload. The grain Reynolds number at x_{end} is twice as large for GWK than for the two medium-scale models. The critical Reynolds numbers for GWK, UNSW and UQ are 4.7, 5.1 and 4.2 respectively. This indicates a lack of transport potential at the x_{end} cross-shore locations (depths) for UNSW and UQ.

As explained in Section 3.2, the sequence of water level increases was different for each experiment. The water level for UQ was increased in a single large step, while in the other two experiments the water level was increased in small incremental steps. Although the sudden increase in depth at UQ affects the wave orbital velocity at x_{end}, the U_{max} (0.1693 m/s) remains larger than the critical orbital velocity required to initiate motion U_{crit} (0.1267 m/s), hence the Shields's number at the higher water level (0.0773) is still higher than the critical threshold for bedload transport (0.0403). The incremental steps in GWK and UNSW have a smaller impact on the orbital velocity and Shields's number at x_{end}. The total water level increase is noted Δh and, divided by the significant wave height H_s, gives the water level increase relative to the wave height for each experiment (Table 3). For GWK and UNSW, the total water level rise corresponds to 50% of the wave height whereas it is only 31% for UQ.

In summary, GWK and UNSW are distorted with respect to physical geometry ($n_g = 1.5$) and Froude scaling law, and thus have different wave steepness. They do not have the same Iribarren number and to a minor extent Dean number. They do not have the same Shields and Reynolds number, implying no suspended sediment transport at the back of the bar for UNSW. They are entirely distorted in scale, however their relative water level rise is identical. On the other hand, GWK and UQ are undistorted with respect to physical geometry scale ($n_g = 1$), but are distorted with respect to the Froude scaling law, and thus have different wave steepness. They also differ in terms of the Iribarren number, and to a

minor extent Dean number. They do not have the same Shields's and Reynolds number, with minimal suspended sediment transport at the back of the bar for UQ. Additionally, the relative water level rises do not match, with GWK being larger than UQ and the UQ water level rise occurring in a single step. The two medium-scale experiments (UQ and UNSW) are fully distorted with respect to each other in terms of all criteria discussed above, except for the Reynolds number. This implies that similar sediment transport and bedform formation is likely to occur on the seaward side of the bar, with a small amount suspended sediment transport for UQ but none for UNSW. UNSW also used a larger relative water level rise than UQ. The value of the Iribarren and Dean numbers are characteristic of erosive conditions for all the experiments, hence an erosive profile is expected to develop. They also have very similar values of the modified version of the Dean number, Ω_β. Given that the experiments are significantly distorted to each other as highlighted by the discussion above, it is not possible to apply any time scaling laws. Instead, the number of waves is used as a relative time.

4.2 Dimensionless profile comparison

It is important to use a suitable method to compare the different profiles from the three distorted experiments. To align experimental profiles along the same slope in dimensionless space, it is necessary to rotate them and plot them relative to a common physical parameter. For this study, this was chosen to be the runup limit, *R,* defined as the vertical elevation not exceeded by any wave run-up measured from the still water line, which is taken as the point at which no changes occur on the sub-aerial beach between consecutive profiles.

Using this parameter instead of *A* in Eq. (4) and Eq. (5) taken from Peregrine and Williams (2001) [21], the local coordinates are converted into dimensionless coordinates as:

$$x^* = \frac{x\ sin\beta}{R} \tag{7}$$

$$z^* = \frac{z\ cos\beta}{R} \tag{8}$$

with β the angle of the initial beach slope, x and z the local coordinates and x^* and z^* the new dimensionless coordinates. Note that in Peregrine and Williams (2001) [21], $R=2A$, so there is a factor two difference in the method presented here compared to the scale presented in Peregrine and Williams (2001) [21]. Other starred symbols used later are also dimensionless.

Before applying these transformations, the coordinate systems of each dataset were set to a common datum, using their respective initial still water shoreline position, such that the initial shoreline position becomes the origin in the new dimensionless space (see Figure 1). Therefore, the three profiles have the same origin for the initial planar slope, with positive values in x^* and z^* indicating landward and above the original shoreline respectively. In addition, the maximum berm elevation should be slightly below $z^* = 1$ for each experiment as the berm is usually built close to the level of the largest run-up events. Eq. (7) and Eq. (8) were developed to enable comparison of profiles of different scales, with minimum disruption to profile shape and conservation of profile perturbations and features.

5. RESULTS

5.1 Beach profile comparison for a fixed water level

5.1.1 Beach profile evolution

Figure 2 demonstrates that despite the differences in experimental procedure described in Section 3.1, the beach profile in each experiment developed a double bar system that moved offshore through time. This is a commonly observed feature in laboratory tests [30, 12, 31, 32] and often on natural coastlines [33, 34, 35, 36]. The profiles are characterised by a dominant outer bar corresponding to the main breakpoint bar for the wave conditions used. The inner bar is smaller, located landward of the outer bar and has a higher crest elevation than the outer bar for all cases. This feature has sometimes been associated with the splash-jet motion of plunging waves pushing material onshore [37]. The trough present between the two bars has a different size and shape for each experiment.

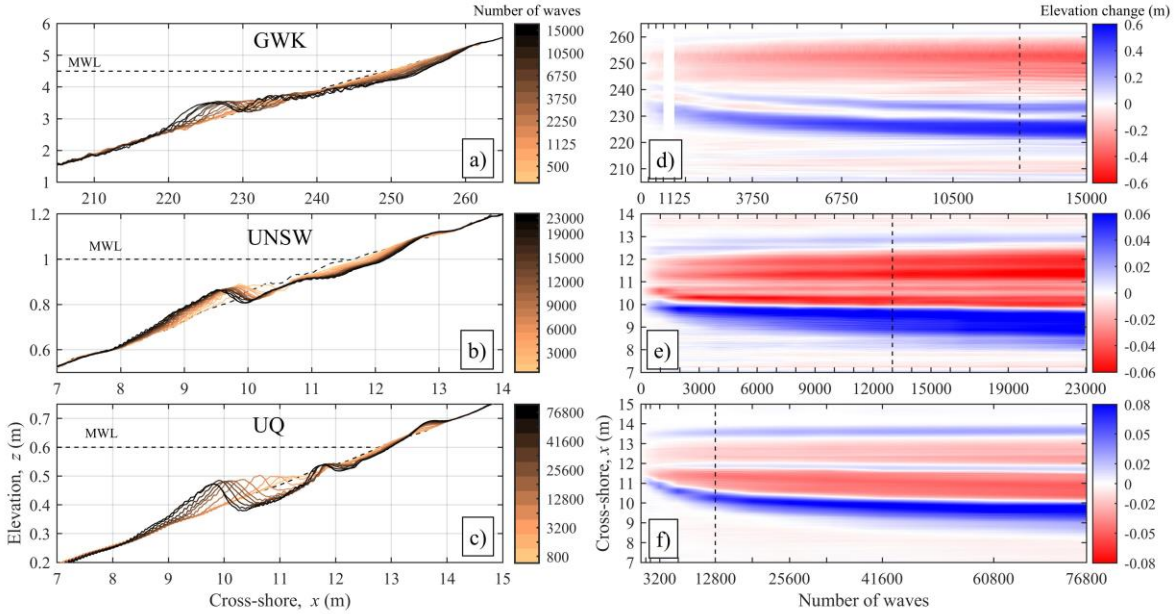

Figure 2: a), b) and c): Beach profile evolution from the initial planar slope to the final profile for GWK (top panels), UNSW (middle panels) and UQ (bottom panels), at their respective initial water level (see Table 3 for more details). The dashed black profile represents the initial planar slope. Each measured profile at the end of each run is associated with a number of waves and is represented from light copper to black. d), e) and f): Beach profile elevation change relative to the initial profile, as a function of the number of waves. Accretion is shown in blue and erosion in red. The vertical black dashed lines indicate the relative moment at which the profile is taken for the comparison, which corresponds to the profile after 12750, 13000 and 12800 waves for GWK, UNSW and UQ respectively. Note that the profiles are shown in their original and respective coordinates system.

All profiles display an accretive berm, but of different size, h_{berm}. The berm developed in the UQ experiment is larger than for the other two experiments. In addition, the inner surf zone for GWK and UNSW features a Low Tide Terrace [29] type profile, with multiple ripples present in the GWK profiles, with a typical ripple length of approximately 1.4 m. This part of the profile is much smaller in cross-shore extent for UQ.

For UQ and UNSW, the outer bar does not have a clearly defined edge. Instead, the bar stretches along the offshore slope with ripples on top. As observed in Baldock et al. (2017) [25], this may be related to the orbital sheet flow which is not strong enough to flatten the bed at this depth in a medium-scale experiment (small Shields and Reynolds number, see section 4.1). The sediment at this depth is assumed to mainly move under bedload transport, with no or limited suspended transport for UNSW and UQ because the Shields number is very close to the threshold for suspension. The bar at GWK is

less elongated and displays a more abrupt offshore edge, characteristic of sheet flow with both bedload and suspended sediment transport. Nevertheless, it seems that the depth of closure for all experiments lies at the seaward limit of the bar, in agreement with the observations of Baldock et al. (2017) [25].

5.1.2 Dimensionless comparison

The scale parameters and the method presented in Section 4.2 (Eq. 7 and Eq.8) were applied for each experiment. The non-dimensional profiles measured after approximately the same number of waves are shown in Figure 3.a, where the value of R (the vertical elevation at x_0, where zero bed-level change was measured) for each experiment was measured at z = 1.020 m for GWK, z = 0.137 m for UNSW and z = 0.095 m for UQ. Note that the ratios of the distance between the bar and the shoreline and the distance between the shoreline and the berm are conserved through this transformation (and relative distances are conserved in general).

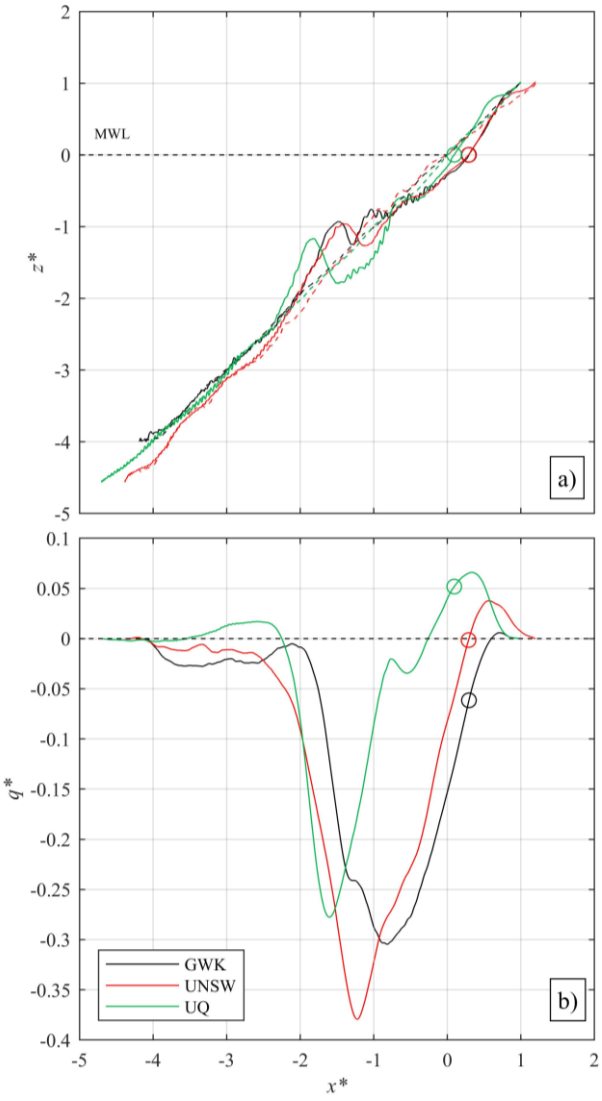

Figure 3: a) Beach profiles in dimensionless space using Eq. 7 and 8. The dashed line represents the initial planar beach slope. The solid lines represent the profile measure after 12750, 13000 and 12800 waves for GWK, UNSW and UQ respectively, for the initial water level. The origin corresponds to the shoreline position for the three initial profiles. b) Dimensionless sediment transport over the active profile. Positive values represent onshore transport and negative values represent offshore transport. For both figures, GWK is in black, UNSW is in red and UQ is in green. The circles mark the shoreline position in each experiment, following the same colour pattern.

Figure 3.a shows that beyond the general qualitative similarity (double bar system and berm) presented in section 5.1.1, the relative lengths of the profiles are consistent. The GWK and UNSW profile are very similar with respects to the bar and berm location (although the shape is different), beach face erosion and shoreline position while for the UQ profile, these features are further seaward. The berm is located below $z^* = 1$ for each profile (below the measured *R)* and the berm formed is larger for the two medium-scale experiments than for the prototype. The beach face steepens with erosion for all the experiments.

The values of the modified version of the Dean number are very similar between experiments, as discussed and shown in Table 3. Therefore, although there was no attempt to follow any hydrodynamic scaling rules between these experiments (Section 4.1), they are expected to reach the same beach profile state in the Wright and Short (1984) [29] classification. As a consequence, the development of the bar follows the same trend for the three experiments, as shown in Figure 4. This figure uses the approach from Eichentopf et al. (2018) [32] which consists of plotting the bar height, h_{bar} as a function of the bar location, x^*_{bar} with both values normalised by their final position. Note that this normalisation was performed with the profiles scaled in the dimensionless space. Figure 4 displays three lines with the same gradient, suggesting that the seaward movement of the bar and its height during the profile formation are consistent between experiments. A similar trend was also observed in Eichentopf et al. (2018) [32], with profiles obtained from experiments with a value of Ω_β similar to the current experiments ($\Omega_\beta = 0.24$). The main differences between these profiles are the cross-shore position and elevation of the inner bar, as well as the size of the trough which is deeper and wider for UQ and UNSW than for GWK.

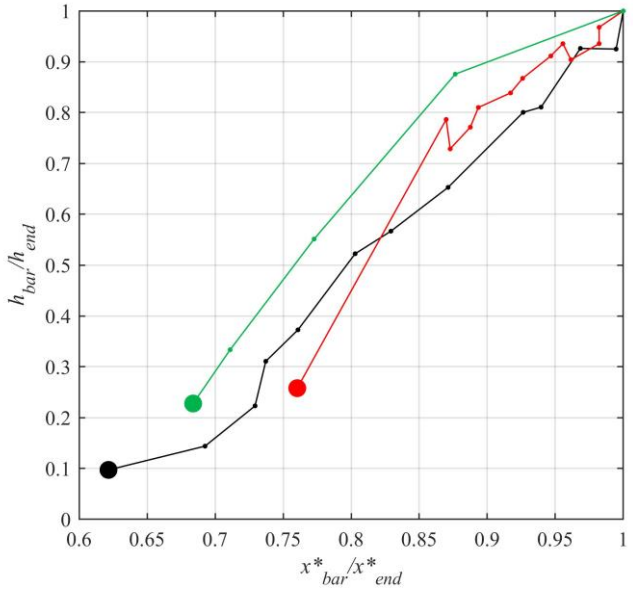

Figure 4: Bar height, h_{bar} evolution as a function of the dimensionless cross-shore bar position, x^*_{bar}. Both values are normalised by their position after 12750, 13000 and 12800 waves for GWK (black), UNSW (red) and UQ (green) respectively, for the initial water level. The large dots mark the initial value. Note that the lines are going to the right, which indicates offshore movement.

Figure 3.b shows the dimensionless sediment transport q^*, calculated between the profiles shown in Figure 3.a, using Eq. (6). The transport was calculated from $x = x_0$, where no profile change was measured on the sub-aerial beach between consecutive profiles (corresponding to *R*), to the seaward end of the active profile x_{end}. The closure errors were corrected as explained in Section 3.3. Positive values correspond to onshore sediment transport and negative values to offshore sediment transport. This parameter is considered as the key parameter to assess the degree of comparability between experiments, as similarities in the pattern and magnitude of sediment transport largely contribute to the overall qualitative comparability of the profiles. Figure 3.b globally shows very similar dimensionless cross-shore sediment transport curves in all three cases. The scaled and prototype models have a peak

transport rate within a factor of 1.4. However, minor differences persist as onshore sediment transport is larger for the two medium-scale experiments than for the prototype, which explains the larger berm in these cases. Furthermore, the position of the shoreline relative to the berm differs for each experiment. For the UQ experiment the shoreline is situated in a region of onshore transport near the top of the berm, whereas it is located in a region of offshore sediment transport in the GWK; and at the beach pivot point for UNSW. Note that because of closure errors, there are some uncertainties in the direction of the sediment transport and magnitude seaward of x* = -3. The other qualitative difference is in the respective location of the maximum offshore transport. This peak occurs at $x^* = -0.9$ for GWK, which corresponds to the trough of the inner bar. For UNSW and UQ, it is observed at $x^* = -1.2$ and $x^* = -1.6$ respectively, corresponding to the trough of the outer bar. This is likely due to the larger value wave steepness in the medium-scale models, resulting in waves breaking relatively further offshore for UNSW and UQ than for GWK.

The application of the new scaling approach allowed the three distorted experiments to be compared. The general profile shape, bar behaviour and most importantly, the sediment transport pattern have shown good agreement between the experiments. However, while these distorted models are qualitatively comparable, it is clear that an erosive condition cannot be compared with an accretive condition. Therefore, only experiments expected to develop a similar profile shape under a comparable sediment transport pattern can be quantitatively compared together, using this scaling method. By looking at the morphological parameters presented in Table 3, it then appears that the modified version of the Dean number (Ω_β) should closely match between the experiments (distorted or not) to be selected.

5.2 Analysis of the method and additional datasets

5.2.1 Validation of the scaling method with additional datasets

The methodology presented in this paper was developed using the three distorted experiments presented above. However, this method would ideally be applicable for all laboratory datasets with similar overall profile forcing and response (*i.e.*, erosive or accretive), thus enabling the scientific community to quantitatively compare distorted models. For this purpose, it is important that all experiments have comparable values of the modified version of the Dean number (Ω_β). In this section, two additional flume datasets with similar values of Ω_β are analysed and compared:

- SANDS Data CIEM, obtained at the Canal d'Investigació i Experimentació Marítima (CIEM) of the Universitat Politecnica de Catalunya (UPC) in Barcelona, Spain [38];
- CRIEPI Data (L5), obtained in the Large Wave Flume (LWF) of the Central Research Institute of Electric Power Industry, Japan, in 1996 [39].

Table 5 shows the main characteristics and parameters for the two additional experiments. The objective here was to use the newly developed scaling method on datasets not used to develop the method, in order to validate it and assess its functionality. There were no attempts to analyse the differences between the experiments further than the profile shape and sediment transport. For this reason, the detailed scale analysis of these two extra datasets is not presented here. It is suggested that one should be able to assess if datasets are comparable using the modified version of the Dean number (Ω_β), and then perform a scaling analysis of the wanted parameters to be compared.

Table 5: Flume size, wave conditions and main parameters for the two extra datasets used in this section.

	Length (m)	**Width (m)**	**Height (m)**	$H_s - H_0$ **(m)**	T_p **(s)**	**Slope**	**Sand** D_{50} **(mm)**	W_{st}	ξ_0	Ω_β
SANDS	100	3	4.5	0.53 – 0.56	4.14	1:15	0.25	0.021	0.46	0.30
CRIEPI (L5)	205	3.4	6	1.20 – 1.27	3	1:10	0.97	0.091	0.22	0.32

The two extra experiments used random waves, with a JONSWAP spectrum. They extend the previous analysis by introducing two intermediate model scales to those already presented, as well as two different sediment grain diameters. While the beach slopes are the same as those analysed previously, these experiments have a smaller (SANDS) and a coarser (L5) sand diameter. For the SANDS experiment, the value of parameters in the three rightmost columns in Table 5 lie between those for GWK and UNSW with the exception of a smaller sediment size. L5 has the largest wave steepness (W_{st}), modified Dean number (Ω_β), and sediment size (D_{50}), but has the smallest Iribarren number (ξ_0). Figure 5.a and 5.b show the dimensionless profiles after approximately the same number of waves (GWK: 12750, UNSW: 13000, UQ: 12800, SANDS: 12500, and L5: 12600).

The SANDS profile closely matches the GWK profile, with very similar bar locations and elevations, trough size, berm height and elevation and beach face slope. The offshore sediment transport peak is located at the same relative position as for GWK (Figure 5.b) — at the inner bar trough — which can here also be related to the relatively small wave steepness W_{st}. In contrast, the onshore sediment transport around the berm is closer to that for the UNSW dataset.

The L5 profile is similar in shape to that for UQ, with a large trough and a small value of ξ_0. However, although the sand is relatively coarse, the berm height is among the smallest. This is confirmed by the weak onshore sediment transport around the berm area (Figure 5.b). The offshore sediment transport peak is located at the same relative position as for UNSW and UQ — at the outer bar trough — which is also related to a high wave steepness.

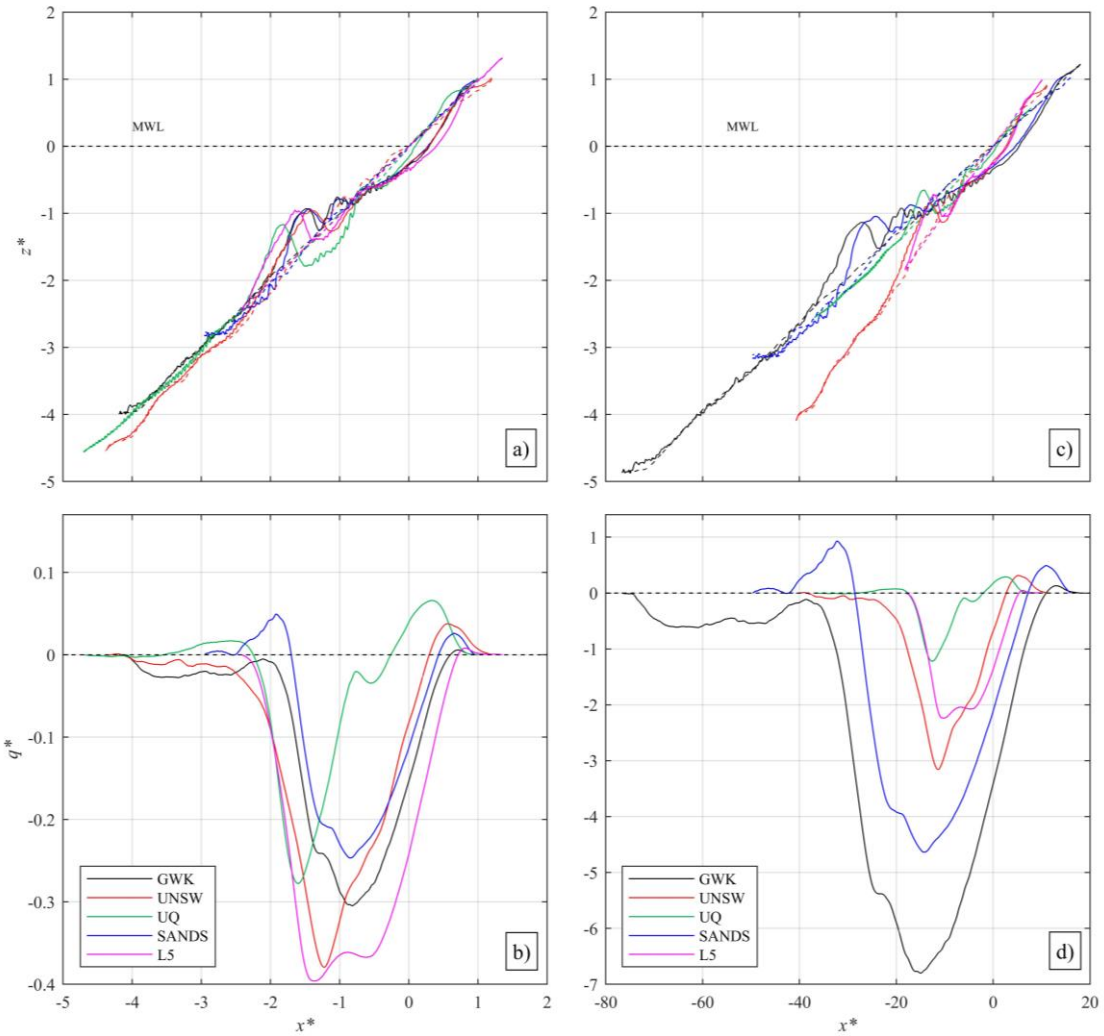

Figure 5: a) Beach profiles in dimensionless space using Eq. (7) and (8) and c) beach profiles in dimensionless space normalised by $H_{m0,}$ from Van Rijn et al. (2011) [2]. The solid lines represent the profile after 12750 (GWK), 13000 (UNSW), 12800 (UQ), 12500 (SANDS) and 12600 (L5), for still water level. Note that for better clarity, the initial planar profiles are not shown. The origin corresponds to the shoreline location for the three initial profiles. b) dimensionless sediment transport over the active profile scaled using Eq. (7) and (8) and d) dimensionless sediment transport over the active profile scaled using H_{m0}^2, from Van Rijn et al. (2011) [2]. Positive values represent onshore transport and negative values represent offshore transport. For all figures, GWK is in black, UNSW is in red, UQ is in green, SANDS is in blue and L5 is in magenta.

5.2.2 Analysis of the new scaling method

In this section, the scaling method is analysed using only the three original datasets. By scaling the coordinate system with R in Eq. (7) and (8), the sediment transport per unit width (i.e., x^* times z^*) scales with $cos\beta.sin\beta/R^2$. As a result, sediment transport is scaled by a factor of 0.0638, 5.1050 and 7.8743 for GWK, UNSW and UQ respectively. This gives a factor of 123 for the sediment transport rate between GWK-UQ, 80 between GWK-UNSW and 1.5 between UNSW-UQ. For future use of equations 7 and 8 when the elevation of zero beach change is not available for each profile, a predicted value of $R_{2\%}$ can be used instead. In this study, similar results to those presented in Figures 3 and 5 were obtained by estimating $R_{2\%}$ using the run-up equation developed by Blenkinsopp et al. (2016) [40] (Eq. A.1). Therefore, it is suggested that predicted $R_{2\%}$ can be used as a substitute for R, using the best run-up equation available for each study site, in order to align the berm position near $z^* = 1$.

The approach of Ibrahim and Baldock (2020) [41] is used to relate the scaling based on R to the offshore wave conditions. This involves rewriting the Peregrine and Williams (2001) [21] solution for swash overtopping in terms of H, L_0 and $\tan\beta$. Taking the most widely applicable runup scaling as that due to Hunt (1959) [42], R is typically proportional to $(H_0L_0)^{1/2}\tan\beta$. Therefore, from Eq. (4) and (5), the sediment transport per unit width scales with $H_0L_0\tan\beta$ (ignoring a factor $\cos^2\beta$ which is almost equal to 1 for all realistic beach slopes). This gives a factor of 128 for the sediment transport rate between GWK-UQ, 84 between GWK-UNSW and 1.5 between UNSW-UQ, which are close to those obtained with measured values of R While the two medium-scale models have almost identical values of H_0L_0 (~0.37), the different beach slopes introduce a scale factor of 1.5 on the dimensionless transport. This is consistent with the additional factor of $\tan\beta$ introduced into the Dean parameter by Hattori and Kawamata, (1980) [17] (Table 1).

Van Rijn et al. (2011) [2] performed a similar comparison of profiles and volumes of sediment transport between three undistorted large-scale laboratory experiments. They used the factor H_{m0} to non-dimensionalise the profile, and H_{m0}^2 to non-dimensionalise the volume of sediment transport. Figure 5.c shows the same profiles as in Figure 5.a but non-dimensionalised using H_{m0} as per Van Rijn et al. [2]. Using this scaling method, the similarity between profiles is less than that observed in Figure 5.a. The shape of the profiles and the relative positions of the main morphological features are quite different for all experiments (see Table 6) with dissimilarity in terms of slope, beach profile length and height, and therefore bar and berm elevation and position. According to the Van Rijn et al. [2] approach, the volume of sediment transport per unit width scales with H_{m0}^2, hence by a factor of 0.7022, 0.0234 and 0.0289 for GWK, UNSW and UQ respectively, which gives a ratio of only 24 between GWK-UQ, 30 between GWK-UNSW and 1.2 between UNSW and UQ. Figure 5.d shows this result, demonstrating very different non-dimensional offshore transport rates between models and prototype experiments. In addition, the onshore sediment transport component is also distorted and does not relate to the size of the observed berm. For distorted models, it is therefore suggested that scaling with the runup (which incorporates H, L and β, and hence Iribarren number) is more appropriate than using just the wave height. Interestingly, Pujara et al. (2020) [43] show that swash backwash flows also scale with HL, and backwash flows could be expected to have a significant influence on sediment transport rates and erosion on the upper beach.

5.2.3 Analysis of the scaled profiles and parameters

The scaling method developed here enables the original coordinates – which significantly differ from one experiment to another due to the wide range of flume sizes – to be scaled in the same dimensionless space. Table 6 presents four measurements in original coordinates, in dimensionless space using the method presented in this paper (Figure 5a), and using the Van Rijn et al. (2011) [2] scaling (Figure 5b) for the five datasets presented in Figure 5. Measurements in the original coordinates vary depending on the size of the flume, however when the new scaling method is used, these measurements scale to comparable values. For the present data, in the new dimensionless coordinates, the bar depth is approximately equal to 1 (*i.e.*, similar to the run-up elevation), the berm elevation (z_{berm} on Figure 1) is around 0.9 (*i.e.*, near the vertical runup limit) and the horizontal distance between the bar crest and the berm crest only varies from 2.29 to 2.51. This confirms that experiments with a similar modified Dean number can be scaled and compared using the scaling method presented, regardless of the original size of the flume or sediment diameter. By contrast, the same analysis performed with Van Rijn et al. (2011) [2] scaling gives a larger range of non-dimensional values for the same features, as it does not correct for the slope and uses the wave height H for the horizontal and the vertical scaling. Table 6 suggests that scaling on the runup (*i.e.*, on $\tan\beta$ and $(HL)^{1/2}$) is more appropriate, particularly for distorted models.

Table 6: Comparison of four parameters – bar height (h_{bar}) (see Figure 1), depth of the bar crest (z_{bar}) (see Figure 1), horizontal distance between the bar crest and the berm crest and vertical elevation of the berm crest above the mean water level (z_{berm}) – after 12750 (GWK), 13000 (UNSW), 12800 (UQ), 12500 (SANDS) and 12600 waves (L5). The values are given, from left to right, as: original coordinate / scaled coordinate using the method presented in this paper / scaled coordinate using Van Rijn et al. (2011) [2] scaling.

	Bar height (h_{bar})	**Bar depth (z_{bar})**	**Horizontal Distance Bar - Berm**	**Berm elevation (z_{berm})**
GWK	0.55m / 0.52 / 0.64	0.95m / 0.93 / 1.14	36.4m / 2.29 / 42.07	0.90m / 0.88 / 1.06
UNSW	0.07m / 0.49 / 0.42	0.13m / 0.95 / 0.86	3.46m / 2.29 / 21.17	0.09m / 0.87 / 0.78
UQ	0.06m / 0.67 / 0.38	0.11m / 1.17 / 0.65	3.40m / 2.45 / 19.32	0.07m / 0.82 / 0.45
SANDS	0.33m / 0.51 / 0.56	0.59m / 0.94 / 1.05	21.48m / 2.29 / 38.33	0.56m / 0.91 / 1.00
L5	0.63m / 0.71 / 0.49	0.94m / 0.98 / 0.74	24.00m / 2.51 / 19.13	0.88m / 0.92 / 0.70

As can be seen in Figure 5, for the five experimental datasets analysed, the scaling method presented in this paper produces peak negative values of the sediment transport within a factor of 1.6 (SANDS having the smallest value with $q^* = -0.25$ and CRIEPI the largest with $q^* = -0.40$). In contrast, the scaling from Van Rijn et al. (2011) [2] gives peak values within a factor of 7. Further, the total bulk sediment transport volume [25], as defined in Section 3.3, is also well scaled with the current method. Figure 6 shows the values of the bulk sediment transport for the five datasets, obtained using the current scaling (black bar, left-hand side axis) and the Van Rijn et al. (2011) [2] scaling (red bar, right-hand side axis). The range of the bulk sediment transport is smaller using the proposed scaling method, with values varying from 0.27 (UQ) to 0.74 (CRIEPI) (*i.e.*, within a factor 3), while for the Van Rijn et al. (2011) scaling, the bulk transport ranges over a factor of 20. However, while the total bulk sediment transport is more uniformly scaled with the presented method, values still differ between the five experiments. This is expected, as the modified Dean numbers are not exactly the same and the number of waves is not exactly the same for each experiment, however without more data on the detailed hydrodynamics (wave velocity and instantaneous sediment transport) of each experiment, it is hard to attribute the quantitative differences to specific parameters. Nonetheless, and as stated throughout the paper, the sediment transport patterns are very similar, and thus a qualitative comparison is considered valid, without comparing absolute values (see the Appendix).

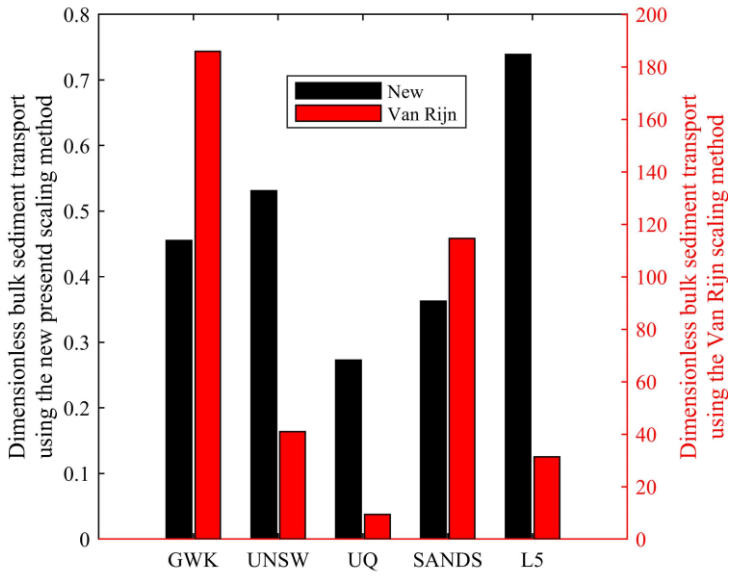

Figure 6: Bar chart showing the bulk sediment transport volume in dimensionless space, using the new scaling method (*left-hand side axis*) and the Van Rijn et al. (2011) [2] scaling method (*right-hand side axis*), measured after 12750 (GWK), 13000 (UNSW), 12800 (UQ), 12500 (SANDS) and 12600 waves (L5). Note the difference in range between the left and right-hand side axes.

The parameters used in the scaling analysis (see Table 3) of each experiment are also scaled and brought into dimensionless space. As a result, the wave steepness is scaled by $tan\beta^{-1}$, the Iribarren number by $tan\beta^{1/2}$ and H_0 by $cos\beta / R$. By contrast, by scaling with H_{m0}, the Van Rijn et al. (2011) [2] method keeps the values of the Iribarren number and wave steepness unchanged, while it squares the wave height. To confirm that the scaled profiles and hydrodynamics are still representative and do not generate artificial features, it is important to compare them with known observations. Figure 7a shows the bar depth (z_{bar}) as a function of H_0^*, and shows that the bar depth increases with wave height when using the current scaling. Assuming that the bar depth corresponds to the average depth of wave breaking, this relationship is in line with the characteristics of wave breaking [44]. However, this relationship is not captured when using Van Rijn et al. (2011) [2] scaling. Furthermore, Figure 7b shows that the ratio $\gamma^*=H_0^* / z_{bar}^*$ is proportional to the wave steepness when using the presented scaling, while it is not with Van Rijn et al. (2011) [2] scaling. As H_0 is proportional to H_b, and assuming that z_{bar} corresponds to the average depth of wave breaking, the ratio H_0^* / z_{bar}^* is related to the breaker index and therefore, as presented in Robertson et al. (2013) [44], proportional to the wave steepness. The scaled profiles and hydrodynamics respect the general relationships of coastal engineering and are therefore, assumed to be valid for further analysis. It is worth noting again that z_{bar}^* (z_{bar}/R) has a smaller range than $\gamma^*=H_0^* / z_{bar}^*$, which is consistent with the wavelength being relevant, and possibly a useful predictor with further testing.

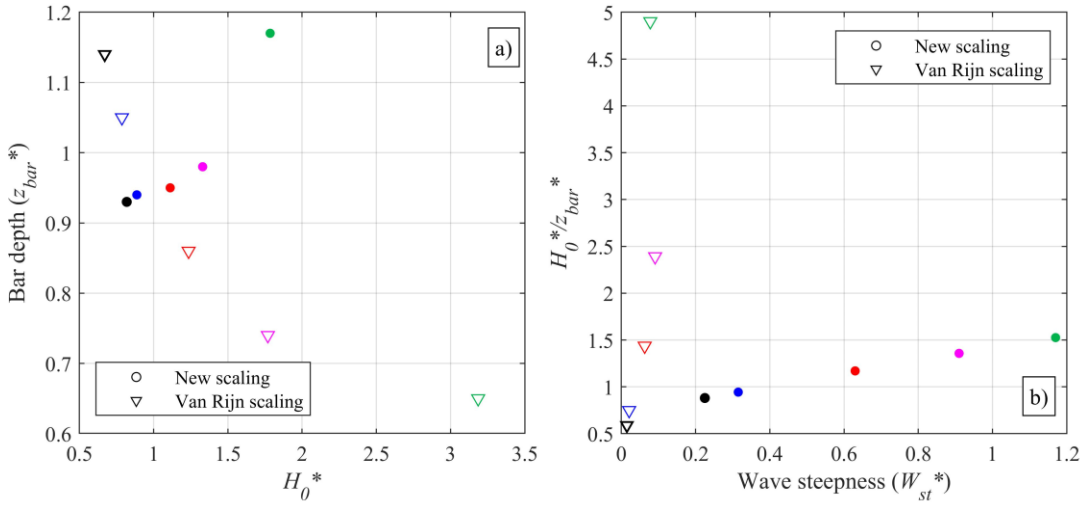

Figure 7: (a) Bar depth (z_{bar}^*) as a function of the deep water significant wave height (H_0^*), in dimensionless space. (b) Deep water significant wave height over bar depth (H_0^*/z_{bar}) as a function of the wave steepness (W_{st}^*) in dimensionless space. On both figures, circles show the values using the new scaling method while the triangles show the values using Van Rijn et al. (2011) [2]. Values were measured after 12750 (GWK, in black), 13000 (UNSW, in red), 12800 (UQ, in green), 12500 (SANDS, in blue) and 12600 waves (L5, in magenta).

5.3 Beach profile comparison with increasing water level

5.3.1 Beach profile evolution

In this section, the new scaling method is extended for profile comparison under increasing water level using the three original datasets. Figure 8.a-c show the beach profile at the end of each water level increment for each of the three experiments. As explained in Section 3.2, the water level was increased in 4 and 5 incremental steps for GWK and UNSW respectively, while for UQ the water level was raised by one large step. Figure 8.d-f show the bed-level changes relative to the initial planar slope (blue marks accretion and red erosion), as a function of the number of waves.

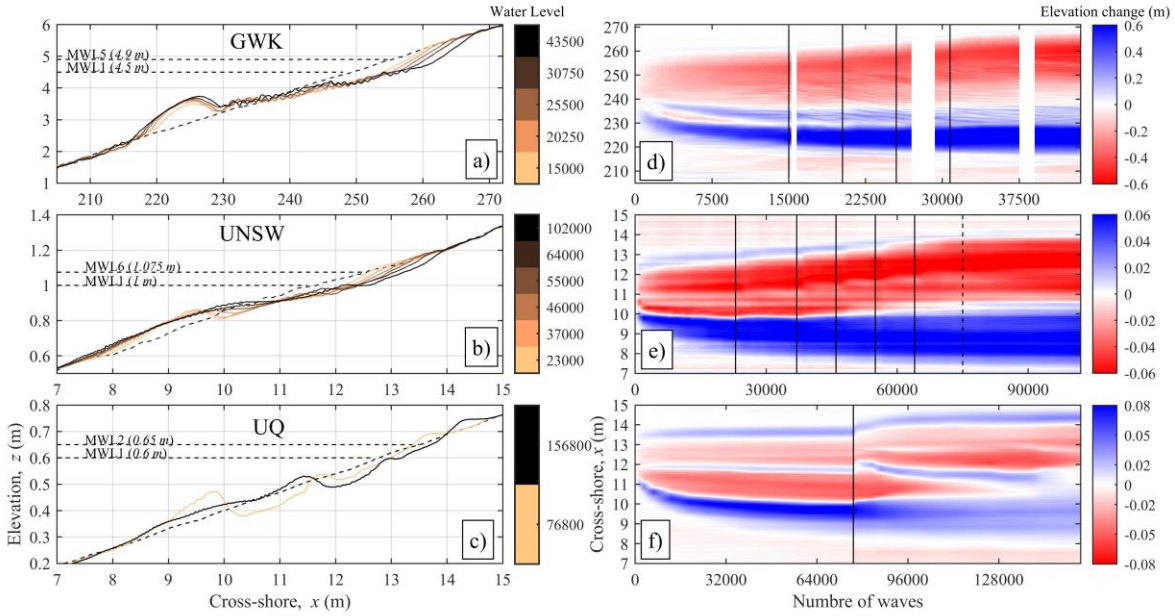

Figure 8: a), b) and c): Beach profile evolution under water level rise. The final profile for each water level increment is shown for GWK (top panels), UNSW (middle panels) and UQ (bottom panels) (see Table 3 for more details). The dashed black profile represents the initial planar slope. Then each measured profile at the end of each water level (and the corresponding number of waves) is represented by a colour, from light copper to black. d), e) and f): Beach profile elevation change relative to the initial planar profile, in function of the number of waves. Accretion is shown in blue and erosion in red. The times at which the water level was increased are shown using a vertical black line. The vertical black dashed line on e) marks the UNSW profile used for the dimensionless comparison.

UQ does not behave similarly to the other two experiments. Indeed, it can be seen on figure 8.f that while the initial outer bar fades away, the initial inner bar moves offshore and becomes a secondary outer bar. Meanwhile, a secondary inner bar is formed. In contrast, GWK and UNSW retain their initial bar which becomes wider and attaches to the inner bar. As observed by Swart (1974) [45] and Atkinson et al. (2018) [6], the cyclic behaviour of the bars observed at UQ can be common in laboratory flume experiments when a very large number of waves is run, highlighting the fact that equilibrium is likely impossible to reach. Furthermore, this behaviour may also represent another aspect of the *morphological hysteresis* presented in Baldock et al. (2017) [25], who showed that the morphological response of a profile is directly linked to the active beach state for the new hydrodynamic conditions. In the current study, this behaviour is mainly observed in the UQ dataset where the large single step water level rise suddenly increases the water level above the initial outer bar, stranding the outer bar, and thus reduces the wave orbital velocity at the bar and makes the inner surf zone more reflective. In addition, the ratio of total water level increase to significant wave height ($\Delta h/H_s$) for UQ (0.3) differs from GWK and UNSW (0.5). This introduces an additional geometrical distortion and further distorts the Froude scaling. For these reasons, the profile obtained at UQ is considered to be too different from the others, and therefore it is not used in the following comparison for an increasing water level.

The profile evolution for GWK and UNSW initially appear quite different, especially around the outer bar area. The UNSW bar seems to decay and becomes relatively larger than the GWK bar. This is mainly due to the weak orbital velocity on the seaward side of the bar for UNSW, which decreases further with water level rise. The area between x = 8 m and x = 9 m is assumed to be dominated by bedload transport (see Section 4.1) for the initial water level. As the water level is raised, the bed shear stress at this location likely decreases and approaches the critical shear stress value, and therefore, a large part of the outer bar volume cannot be transported onshore. This weak transport is also enhanced by the larger sediment used at UNSW. However, to a lesser degree, the widening of the outer bar is also observed at GWK.

Further investigation suggests that similar and comparable qualitative behaviours are observed in both experiments under water level increase. First of all, the shoreline was eroded as the berm retreated, and the bar moved landward and upward as the water level was increased. In both cases, the length of the profile, calculated from the bar crest to the berm crest, increases with the water level rise. From the end of the initial water level to the end of the final water level, the profile length increases by 48 cm (from 3.41 m to 3.89 m) for UNSW and by 5.54 m (from 36.30 m to 41.84 m) for GWK, which corresponds to an increase of 14.2 % and 15.2 % in length for UNSW and GWK respectively. Therefore, it appears that the profiles became more dissipative as the water level was raised, with the shoreline retreating faster than the bar. This behaviour was also observed in Atkinson *et al.* (2018) [6]. The berm elevation, z_{berm} also increases in both experiments, by 2 cm and 4.5 cm for GWK and UNSW respectively. On the other hand, the berm height, h_{berm} remains constant throughout both experiments, suggesting it is approximately self-similar at each water level. Figure 8.d and 8.e show a less distinct inner bar as the outer bar moves landward and attaches to it, making the trough less pronounced. However, Figure 5.a and 5.b still show the presence of an inner bar at x = 245 m for GWK, and x = 12 m for UNSW at the final water level, located upward and landward of their initial position.

5.3.2 Dimensionless comparison

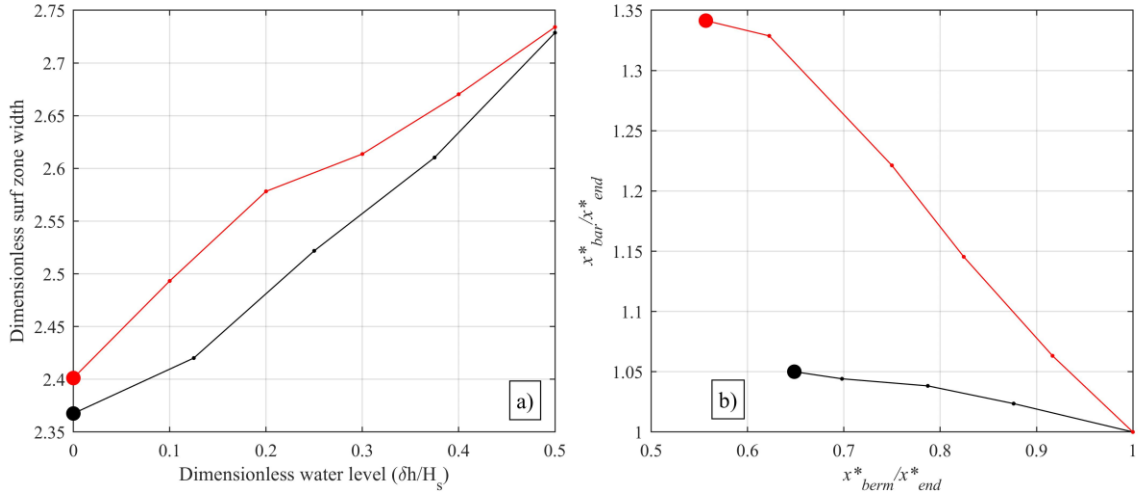

Figure 9: a) Evolution of the dimensionless surf zone width against the dimensionless water level ($\Delta h/H_s$). Note that UNSW (red) had 5 steps while GWK (black) had 4. b) Cross-shore position of the bar as a function of the cross-shore position of the berm, both normalised by their final value. The large dots mark the initial value.

Figure 9.a confirms the observations made in section 5.3.1, showing that the dimensionless width of the surf zone, from the bar to the berm, increases with a very similar gradient for both experiments. To ensure a valid comparison at each water level, the values were taken from profiles measured after approximately the same number of waves at that water level. In Figure 9, it is observed that while the surf zone lengthens at the same rate (Figure 9.a), the pace of the bar and berm retreat differs between the two experiments (Figure 9.b). Except for the first water level increment, where the berm and bar retreat are very similar between UNSW and GWK, UNSW is characterised by a larger retreat of the bar and berm than GWK. This is likely to be, in part, a consequence of the large number of waves run at each intermediate water level at UNSW. This pattern is also visible on the dimensionless profile comparison plotted in Figure 10.a. Note that the final water level in each experiment is not shown in Figure 10.a as it would be at different elevations in the dimensionless space. As such, the elevations of the various profile perturbations cannot be compared directly as they are relative to a different water level and wave conditions for each experiment, hence only the trend is compared. In addition to the previous observations, it is noted that the trough length for UNSW is consistently longer than that for GWK.

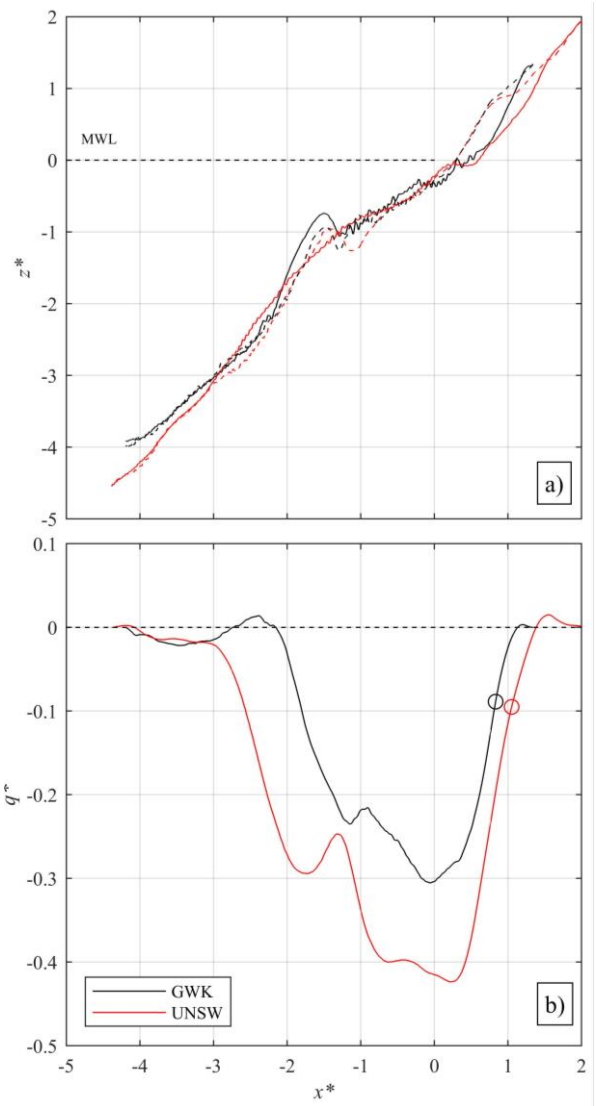

Figure 10: a) Beach profiles in dimensionless space. The dashed lines represent the profiles at the end of the initial water level. The solid lines represent the profiles measured after 10700 waves at z_{wl} = 4.9 m (final water level, GWK) and after 11000 waves at z_{wl} = 1.075 m (final water level, UNSW). The origin corresponds to the shoreline location of the three planar profiles. b) dimensionless sediment transport over the active profile. Positive values represent onshore transport and negative values represent offshore transport. For both figures, GWK is in black and UNSW is in red. The circle marks the final shoreline position in each experiment.

Overall, although the beach profile shape is very different, the behaviour of the profile under water level increase is similar for GWK and UNSW, with the profile lengthening while moving upward and landward, and the berm height being maintained. Although more waves were run at UNSW, the scaled sediment transport curves of the two experiments are very similar (Figure 10.b). As in Figure 3, Figure 10.b shows that the onshore transport around the berm is smaller for the prototype than for the medium-scale model. However, the shoreline is located in a region of offshore sediment transport in both cases. The inner surf zone is still dominated by offshore sediment transport for all experiments. The maximum offshore transport occurs between x^* = 0.5 and x^* = -0.7 for UNSW, and x^* = 0.3 and x^* = -0.1 for GWK, which corresponds to the area of inner bar trough on the dashed profiles for both experiments. Overall, the UNSW and GWK transport rates show a similar pattern with peaks in transport rate occurring at similar cross-shore locations. The sediment transport magnitude is within a factor of 1.4, as for the fixed water level case. The total dimensionless bulk sediment transport values are 0.64 (GWK) and 0.82 (UNSW), which are similar but confirms that they cannot be directly compared. The very similar trends are considered comparable, however, as demonstrated in the Appendix.

6. DISCUSSION

6.1 Constraints associated with the new scaling method

The approach developed in this paper allows distorted experimental profiles with similar modified Dean number (Ω_β) to be compared. This parameter indicates evolution to a similar beach state and to a certain extent, a comparable dimensionless bulk sediment transport [12]. From the extended comparison shown in Figure 5, and using the dataset from Van Rijn et al. (2011) [2], it is suggested that the new scaling approach is appropriate for Ω_β values ranging between 0.24 and 0.35 and for intermediate beach states and erosive conditions (random waves). As shown in Figure 5, the new method is able to scale profiles with different initial planar slopes and with a large range of grain sizes, such that the profile shape and local sediment transport pattern can be quantitatively compared. To summarise, the newly developed approach is associated with the following four constraints:

1) Random waves: the methodology is only valid for profiles developed under random waves.
2) Similar modified Dean number: the comparisons presented in this paper focus on profiles developed under similar erosive condition, in order to show the similarities between distorted experiments in terms of profile development and sediment transport. It is assumed that this technique would work for accretive conditions with similar modified Dean number, but this is yet to be experimented and confirmed.
3) Initially planar beach: the datasets compared in this paper all develop from an initially planar slope after approximately the same number of waves. The method works for different initial slopes, such as the Dean profile, as long as the experiments compared have the same type of initial slope.
4) Data available after the same number of waves: for the purpose of the comparison, it was required to have measured profiles available after approximately the same number of waves.

While constraint 1 is fixed, constraint 2 and 3 can vary depending on the dataset compared, and constraint 4 is more a practical constraint for the comparison – i.e., the number of waves represents equivalent dimensionless time. Existing and future datasets can therefore be compared together, as long as they are consistent with these constraints.

While profiles formed under water level increase in each experiment have a very different shape and did not well matched with this scaling (Figure 10.a), the method still showed good performance in comparing beach profiles behaviour (Figure 9 and 10.b) of distorted flume experiments under water level increase (*e.g.*, profile length increase, sediment transport). In addition to the four constraints above, the additional conditions that need to be respected for the method to be applicable in the case of water level increase are: 1) a similar procedure for the increase of the water level; and, 2) a comparable ratio of the total water level increase over the significant wave height ($\Delta h/H_s$). Note that in this paper, only the progressive incremental steps could be fully assessed and compared. Therefore, further work is required to identify if other matching water level increase procedures are compatible with this method. As for a fixed water level, the method enables a comparison of the profile evolution and sediment transport pattern.

6.2 Application of the new scaling method for a fixed water level

As discussed in Section 5.2.3, the new scaling method proposed in this paper was used to effectively compare beach profiles, sediment transport curves and morphodynamic behaviour from distorted experiments. During this analysis it was observed that the location of the peak offshore sediment transport could be related to the offshore wave steepness (Section 5.1.2 and 5.2.1). As an example application of the new scaling method, this relationship is further analysed in Figure 11. Figure 11 shows that the offshore sediment transport peak location moves further offshore with steeper waves. This can be explained by the fact that steeper waves generate sediment transport further offshore than less steep waves, as for a given depth, the shear stress associated with the orbital velocity is stronger for a

steeper wave. Furthermore, less steep waves tend to break over the trough, as mentioned in Strauss (2009) [46], which explains why the peak of offshore sediment transport is located in the inner bar trough area for GWK and SANDS, but located in the outer bar trough for UNSW, UQ and CRIEPI.

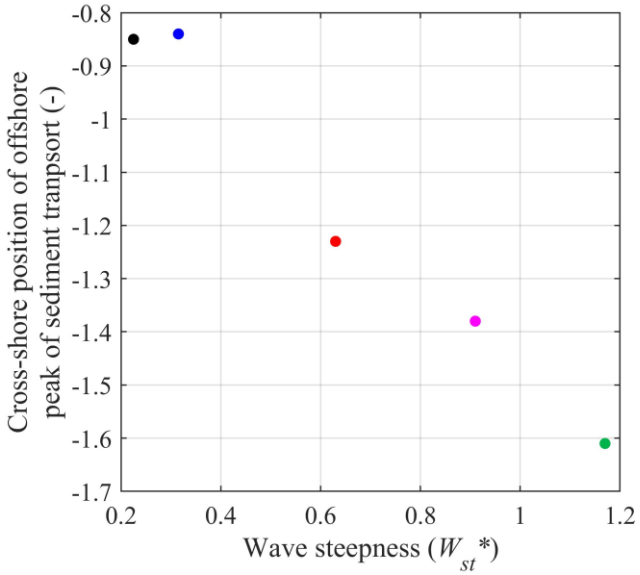

Figure 11: Cross-shore position of the offshore peak of sediment transport as a function of the offshore wave steepness (W_{st}*), in dimensionless space using the new scaling method. Values were measured after 12750 (GWK), 13000 (UNSW), 12800 (UQ), 12500 (SANDS) and 12600 waves (L5). Note that the value is given relative to the initial shoreline for the planar slope in dimensionless space.

7. CONCLUSIONS

Three laboratory flume experiments at different and distorted scales (one prototype (GWK) and two medium-scale (UNSW and UQ)) are reported and compared. These experiments all investigated beach profile evolution under erosive wave conditions and water level rise, with some coastal protection tests under similar conditions performed in the GWK and UNSW experiments. A scale analysis of the hydrodynamics, physical geometry and other key parameters was performed between each experiment. The experiments are distorted with respect to those parameters and also in terms of Froude scaling, Shields's number and Reynolds number. However, they had a very similar modified Dean number.

A novel approach based on the scaling proposed for swash flows by Peregrine and Williams (2001) [21] was applied to transform local coordinates into dimensionless coordinates free of the beach slope, allowing direct comparison of distorted profiles. The comparison of these distorted experiments focused on the analysis of profile shape and development, and mainly on the sediment transport pattern. It demonstrated that as long as the modified Dean number is similar, distorted experiments can be compared using the developed method.

The approach was then validated with two additional datasets which confirmed that the profile shape and sediment transport were suitable for comparison as the peak of erosion occurred around the same relative position, and with the scaled magnitude within a factor of 1.6. The dimensionless coordinates are related to the offshore wave conditions following Ibrahim and Baldock (2020) [41] and with this scaling, the sediment transport scales with H_0L_0, which brings the data into good agreement for profiles exposed to the same number of waves. There is a significant difference between the dimensionless

transport rates, profiles shape and morphodynamics parameters when scaled using this new approach and the conventional approach applicable for the scaling of undistorted profiles (*e.g.,* [2]).

The new scaling method was also applied to tests with increasing water levels. In this case, it was shown that in addition to the modified version of the Dean number, the same procedure for the water level increase and the same relative water level rise are required for a match between the distorted profiles and for the method to be applicable.

APPENDIX

The following analysis presents an example application of the scaling approach developed in this paper for water level increase, using the UNSW and GWK data. As presented in Section 3.2, the GWK and UNSW experiments investigated beach response with a rising sea level on "natural" beaches and beaches with a seawall installed on the upper beach. The DynaRev experiment at GWK investigated the performance of a dynamic cobble berm revetment [8, 23]. The UNSW experiment [7] investigated the influence of a rubble mound and vertical seawall on fronting beach morphology in a rising sea. In both cases, results with a seawall were compared with the case of an equivalent non-engineered sand beach. In this section, erosion volumes are compared for the engineered and non-engineered beaches at two scales by applying Equations (7) and (8). However, as the value of R is hard to obtain on an engineered beach, the equation developed by Blenkinsopp et al. (2016) [40] is used to calculate runup and is defined as:

$$R_{2\%} = 1.165 H_0 \xi_0^{0.77} \tag{A.1}$$

with H_0 the offshore significant wave height and ξ_0 the offshore Iribarren number.

Figure A1 shows the dimensionless volume of sand which was eroded when a seawall structure was present compared to the volume of sand eroded when no structure was placed. The scaling approach allows the volume of erosion in different and distorted scale experiments to be compared, and shows that in all cases the volume of beach erosion with the presence of the protection is close to but smaller than the volume of erosion without the protection for the same wave and water level forcing. To explicitly quantify this effect, a dimensionless "interaction parameter" (*IP*) is defined to quantify the relative interaction between wave run-up and the structure. The *IP* defines the elevation buffer between $R_{2\%}$ and the structure toe, ranging from 0 ($R_{2\%}$ does not reach the structure toe) to 2 (MWL is $R_{2\%}$ above the structure toe) and is defined simply as:

$$IP = \frac{R_{2\%} - (z_{structure} - z_{mwl})}{R_{2\%}} \tag{A.2}$$

where, $R_{2\%}$ is calculated using Eq. (A.1), $z_{structure}$ is the elevation of the structure toe, and z_{mwl} is the elevation of the mean water level. When the shoreline is far from the structure (low *IP*), wave runup is mostly over sand, therefore, the erosion occurs almost as for a beach with no coastal structure present. This is shown by the navy blue points close to the 1:1 line. As the water level increases (higher *IP*), the structure increasingly limits wave runup, hence reducing the area over which sand can be eroded. This is represented by *IP* values in the range 0.7 to 1.8 which lie further below the 1:1 line. Note that the *IP* for GWK dynamic cobble berm revetment is not exceeding 1.2.

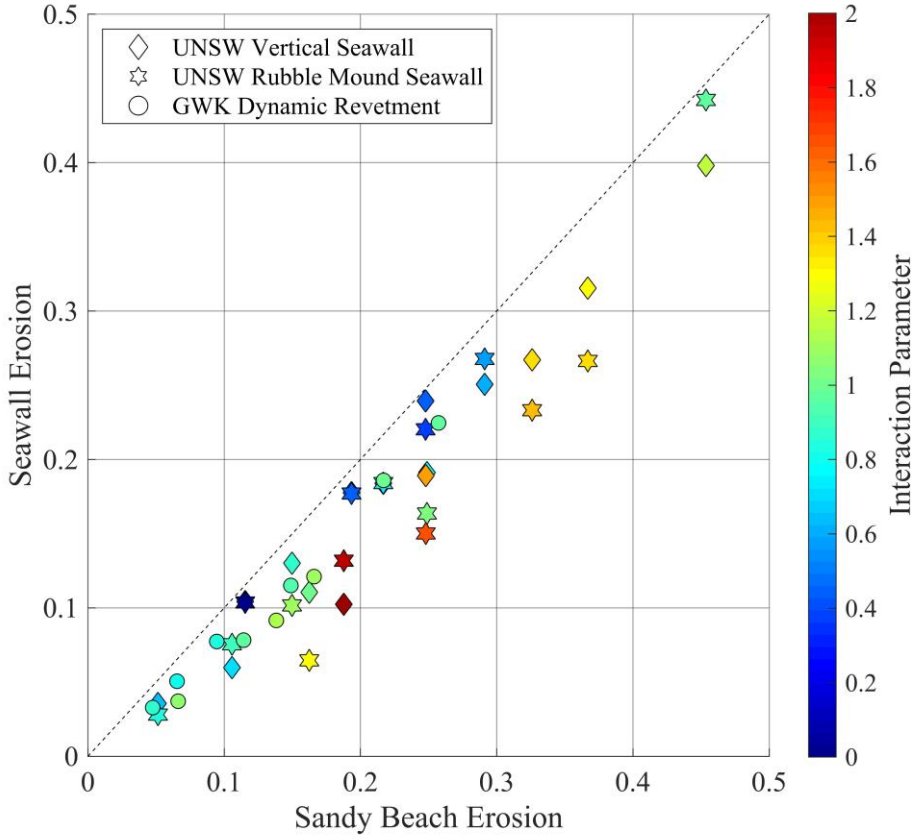

Figure A.1: Dimensionless volume of sand eroded on protected beach versus volume of sand eroded for non-protected beach. The dash black line represents the 1:1 line. Each type of structure is represented by a symbol: Diamonds for UNSW rubble mound seawall; Stars for UNSW vertical seawall; Circles for GWK dynamic cobble berm revetment. A dimensionless interaction parameter (*IP*) was created to account for the relative interaction between wave run-up and the structure.

The above analysis provides an application of the new scaling method and demonstrates that it can be successfully used to quantify the response of a sand beach in the presence of coastal engineering structures on distorted profiles under water level rise, which increases the potential use of existing datasets.

ACKNOWLEDGEMENTS

Funding: The DynaRev project has received funding from the European Union's Horizon 2020 research and innovation programme under grant agreement No 654110, HYDRALAB+. The two medium-scale experiments were funded by an Australian Research Council Discovery Grant, DP140101302. Paul Bayle is supported by a PhD scholarship through the EPSRC CDT in Water Informatics: Science & Engineering (WISE).

The authors gratefully thank Matthias Kudella, Stefan Schimmels, and all staff and technicians from the Großer WellenKanal (GWK) flume for their support before, during and after the DynaRev experiment. They also thanks Iván Cáceres and Sonja Eichentopf for the precious help in the selection of extra dataset for the analysis.

REFERENCES

[1] Hughes, S.A. (1993). Physical models and laboratory techniques in coastal engineering. Advanced Series on Ocean Engineering, Vol. 7. World Scientific, London. 568 pp.

[2] Van Rijn, L.C., Tonnon, P.K., Sánchez-Arcilla, A., Cáceres, I. and Grüne, J. (2011). Scaling laws for beach and dune erosion processes. Coastal Engineering, 58(7), 623-636.

[3] Vellinga, P. (1982). Beach and Dune erosion during storm surge. Coastal Engineering, 6(4), 361-387.

[4] Kraus, N.C., Larson, M. (1988). Beach profile change measured in the tank for large waves 1956-1957 and 1962 (No. CERC-88-6). Coast. Eng. Res. Center Vicksburg MS.

[5] Intergovernmental Panel on Climate Change. (2014). *Climate Change 2013 – The Physical Science Basis: Working Group I Contribution to the Fifth Assessment Report of the Intergovernmental Panel on Climate Change*. Cambridge: Cambridge University Press. doi:10.1017/CBO9781107415324

[6] Atkinson, A.L., Baldock, T.E., Birrien, F., Callaghan, D.P., Nielsen, P., Beuzen, T., Turner, I.L., Blenkinsopp, C.E. and Ranasinghe, R. (2018). Laboratory investigation of the Bruun Rule and beach response to sea level rise. Coastal Engineering, 136, 183-202.

[7] Beuzen, T., Turner, I.L., Blenkinsopp, C.E., Atkinson, A., Flocard, F. and Baldock, T.E. (2018). Physical model study of beach profile evolution by sea level rise in the presence of seawalls. Coastal Engineering, 136, 172-182.

[8] Blenkinsopp, C.E., Bayle, P.M., Conley, D., Masselink, G., Gulson, E., Kelly, I., Almar, R., Turner, I., Baldock, T., Beuzen, T., McCall, R., Reniers, A., Troch, P., Gallach Sanchez, D., Hunter, A., Bryan, O., Hennessey, G., Schimmels, S., Kudella, M. (In review). High-resolution, prototype-scale laboratory measurements of nearshore wave processes and morphological evolution of a sandy beach and dynamic cobble berm revetment. Scientific Data

[9] Noda, E.K. (1972). Equilibrium beach profile scale–model relationship. Journal of Waterways, Harbors and Coastal Division, ASCE WW4, 511–528.

[10] Kamphuis, J.W. (1972). Scale selection for mobile bed wave models. *Proc. 13th ICCE*, Vancouver, Canada, Vol. 2, 1173–1195.

[11] Vellinga, P. (1986). Beach and dune erosion during storm surges. Doctoral Thesis, Delft University of Technology, Delft, the Netherlands (Publication 372, Delft Hydraulics).

[12] Baldock, T.E., Alsina, J.A., Caceres, I., Vicinanza, D., Contestabile, P., Power, H. and Sanchez-Arcilla, A. (2011). Large-scale experiments on beach profile evolution and surf and swash zone sediment transport induced by long waves, wave groups and random waves. Coastal Engineering, 58(2), 214-227.

[13] Alsina, J.M., Sanchez-Arcilla, A., Gironella, X. and Baldock, T.E. (2007). Design of scaled movable bed experiments using numerical models. Journal of Coastal Research, SI 50 (Proceedings of the 9th International Coastal Symposium), 379 – 383. Gold Coast, Australia, ISSN 0749.0208

[14] Baldock, T.E., Manoonvoravong, P. and Pham, K.S. (2010). Sediment transport and beach morphodynamics induced by free long waves, bound long waves and wave groups. Coastal Engineering, 57(10), 898-916.

[15] Gourlay, M.R. (1968). Beach and Dune Erosion Tests. *Report M935/M936*. Delft Hydraulic Laboratory, the Netherlands.

[16] Dean, R.G. (1973). Heuristic models of sand transport in the surf zone. *Proc. Conf. on Engineering Dynamics in the Surf Zone*. N.S.W, Sydney, 208–214.

[17] Hattori, M., Kawamata, R. (1980). Onshore–offshore transport and beach profile change. *Proc. 17th Coastal Engineering Conference*, vol. 2. ASCE, 1175–1193.

[18] Shields, A., (1936) .Anwendung der Ähnlichkeitsmechanik und der Turbulenz Forschung auf die Geschiebebewegung. Mitt. der Preuss. Versuchsamst. für Wasserbau und Schiffbau, Heft 26, Berlin, Deutschland.

[19] Van Rijn, L.C., (1993, 2012). Principles of sediment transport in rivers, estuaries and coastal seas. Aqua Publications, Amsterdam, The Netherlands.

[20] Soulsby, R., (1997). Dynamics of marine sands. Thomas Telford, UK.

[21] Peregrine, D.H. and Williams, S.M. (2001). Swash overtopping a truncated plane beach. Journal of Fluid Mechanics, 440, 391-399.

[22] Guard, P.A., Baldock, T.E. (2007). The influence of seaward boundary conditions on swash zone hydrodynamics. Coastal Engineering, Vol 54, 321-331.

[23] Bayle, P.M., Blenkinsopp, C.E., Masselink, G., Conley, D., Beuzen, T. and Almar, R. (*2020*) Performance of a dynamic cobble berm revetment for coastal protection, under increasing water level. Coastal Engineering, 159.

[24] Atkinson, A. and Baldock, T.E. (2016). A high-resolution sub-aerial and sub-aqueous laser based laboratory beach profile measurement system. Coastal Engineering*,* 107, 28-33.

[25] Baldock, T.E., Birrien, F., Atkinson, A., Shimamoto, T., Wu, S., Callaghan, D.P. and Nielsen, P. (2017). Morphological hysteresis in the evolution of beach profiles under sequences of wave climates - Part 1; observations. Coastal Engineering, 128, 92-105.

[26] Atkinson, A. (2018). Laboratory Beach Profile Dynamics and Responses to Changing Water Levels with and without Nourishment, PhD Thesis, University of Queensland.

[27] Jacobsen, N.G. and Fredsoe, J. (2014). Formation and development of a breaker bar under regular waves. Part 2: Sediment transport and morphology. Coastal Engineering, 88, 55-68.

[28] Battjes, J.A. (1974). Surf similarity. *14th International Conference of Coastal Engineering*, ASCE, 466-480.

[29] Wright, L.D. and Short, A.D. (1984). Morphodynamic variability of surf zones and beaches: a synthesis. Marine Geology, (56), 93-118.

[30] Larson, M. and Kraus, N. (1989). SBEACH: Numerical model for simulating storm-induced beach change. *Technical Report CERC-89-9,* US Army Corps of Engineers.

[31] Masselink, G., Ruju, A., Conley, D., Turner, I., Ruessink, G., Matias, A., Thompson, C., Castelle, B., Puleo, J., Citerone, V. and Wolters, G. (2016). Large-scale Barrier Dynamics Experiment II (BARDEX II): Experimental design, instrumentation, test program, and data set. Coastal Engineering, 113, 3-18.

[32] Eichentopf, S., Cáceres, I. and Alsina, J.M. (2018). Breaker bar morphodynamics under erosive and accretive wave conditions in large-scale experiments. Coastal Engineering, 138, 36-48.

[33] Ruessink, B. G., Coco, G., Ranasinghe, R. and Turner I. L. (2007a). Coupled and non-coupled behavior of three-dimensional morphological patterns in a double sandbar system. Journal of Geophysical Research 112, C07002.

[34] Castelle, B., Bonneton, P., Dupuis, H. and Senechal, N. (2007a). Double bar beach dynamics on the high-energy meso-macrotidal French Aquitanian Coast: A review. Marine Geology 245, 141-159.

[35] Thornton, E., MacMahan, J. and Sallenger, Jr. A. (2007). Rip currents, mega-cusps,and eroding dunes. Marine Geology 240, 151-167.

[36] Turner, I.L., Aarninkhof, S.G.J. and Holman, R.A. (2006), Coastal imaging applications and research in Australia. Journal of Coastal Research, 22, 37-48.

[37] Dette, H.H., Larson, M., Murphy, J., Newe, J., Peters, K., Reniers, A., Steetzel, H. (2002). Application of prototype flume tests for beach nourishment assessment. Coast Engineering. 47, 137–177.

[38] Alsina, J.M., Caceres, I. (2011). Sediment suspension events in the inner surf and swash zone. Measurements in large-scale and high-energy wave conditions. Coast Engineering. 58 (8), 657–670.

[39] Shimizu, T., Ikeno, M. (1996). Experimental study on sediment transport in surf and swash zones using large wave flume. In: 25th International Conference on Coastal Engineering, pp. 3076–3089.

[40] Blenkinsopp, C.E., Matias, A., Howe, D., Castelle, B., Marieu, V. and Turner, I.L. (2016). Wave runup and overwash on a prototype-scale sand barrier. Coastal Engineering, 113, 88-103.

[41] Ibrahim, M.S.I. and Baldock, T.E. (2020). Swash overtopping on plane beaches – reconciling empirical and theoretical scaling laws using the volume flux. Coastal Engineering, Vol 157.

[42] Hunt, I.A. (1959), Design of Seawalls and Breakwaters. Journal of Waterways and Harbors Div., ASCE, Vol. 85, No.WW3.

[43] Pujara, N., Miller, D., Park, Y.S., Baldock, T.E. and Liu, P.L.F., (2020). The influence of wave acceleration and volume on the swash flow driven by breaking waves of elevation. Coastal Engineering, p.103-697.

[44] Robertson, B., Hall, K., Zytner, R. and Nistor, I. (2013), Breaking waves: review of characteristic relationship. Coastal Engineering, 55 (1).

[45] Swart, D.H., (1974). Offshore Sediment Transport and Equilibrium Beach Profiles. Doctoral dissertation. Delft University of Technology, TU Delft.

[46] Strauss, D.R. (2009). Morphological modeling of intermediate beach state transitions. Griffith School of Environment Science, Environment. Engineering and Technology Griffith University.